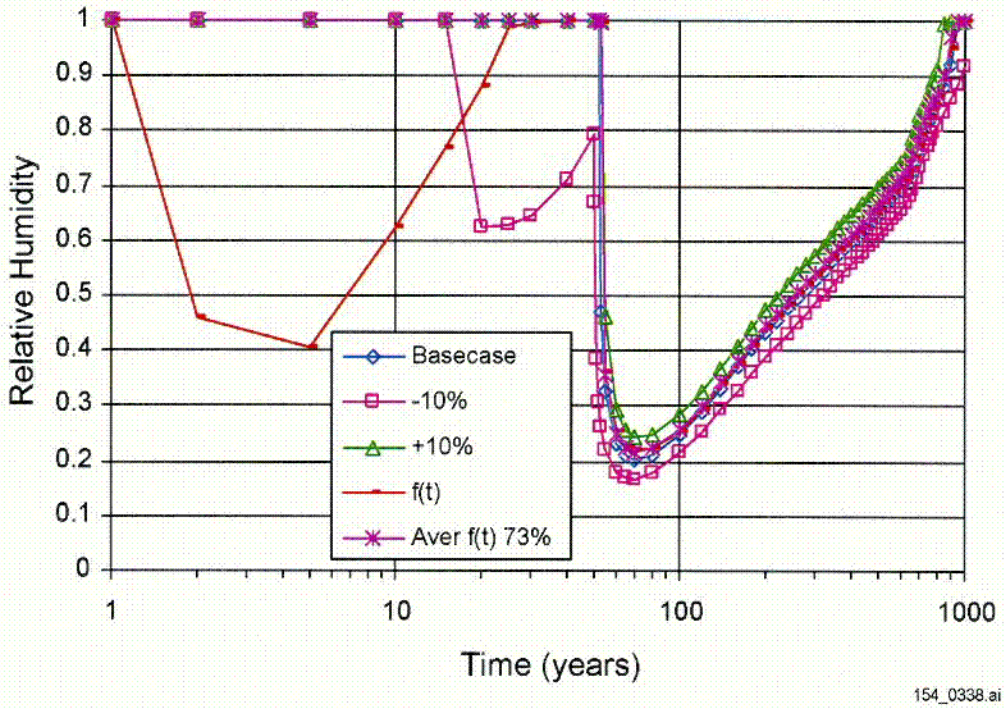

154_0338.ai

Source: Produced using files from Leem 2001 [DIRS 154996].

NOTE: Relative humidity histories presented as a function of ventilation efficiency.

Figure 5.3.2.4.2-6. Drift Wall Crown Relative Humidity Histories for the Higher-Temperature Operating Mode

C01

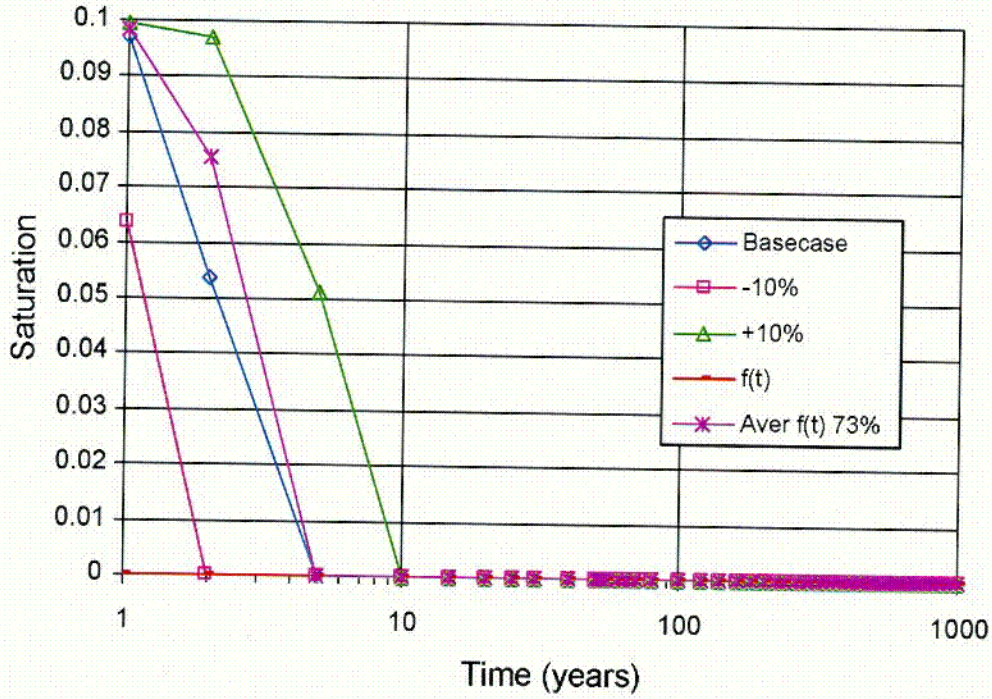

154_0339.ai

154_0339.ai

Source: Produced using files from Leem 2001 [DIRS 154996].

NOTE: Saturation histories presented as a function of ventilation efficiency.

Figure 5.3.2.4.2-7. Invert (Lower Center) Saturation Histories for the Higher-Temperature Operating Mode

C02

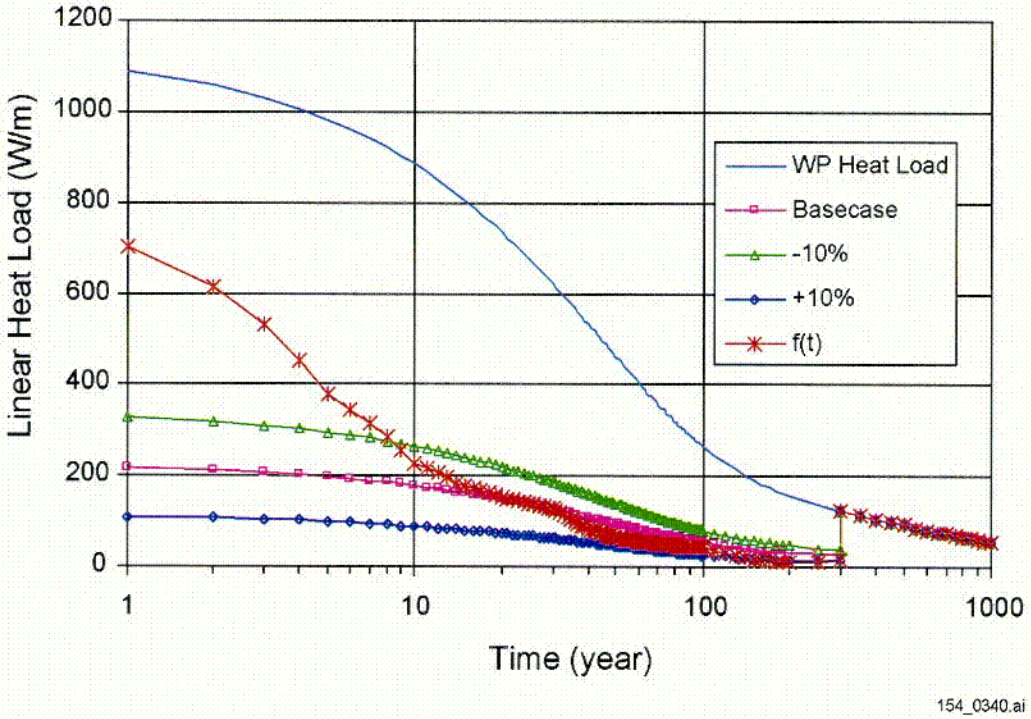

154_0340.ai

Source: Produced using files from Leem 2001 [DIRS 154996].

Figure 5.3.2.4.2-8. Time History of Heat Available to Enter the Near-Field Rock for the Lower-Temperature Operating Mode Ventilation Cases

C03

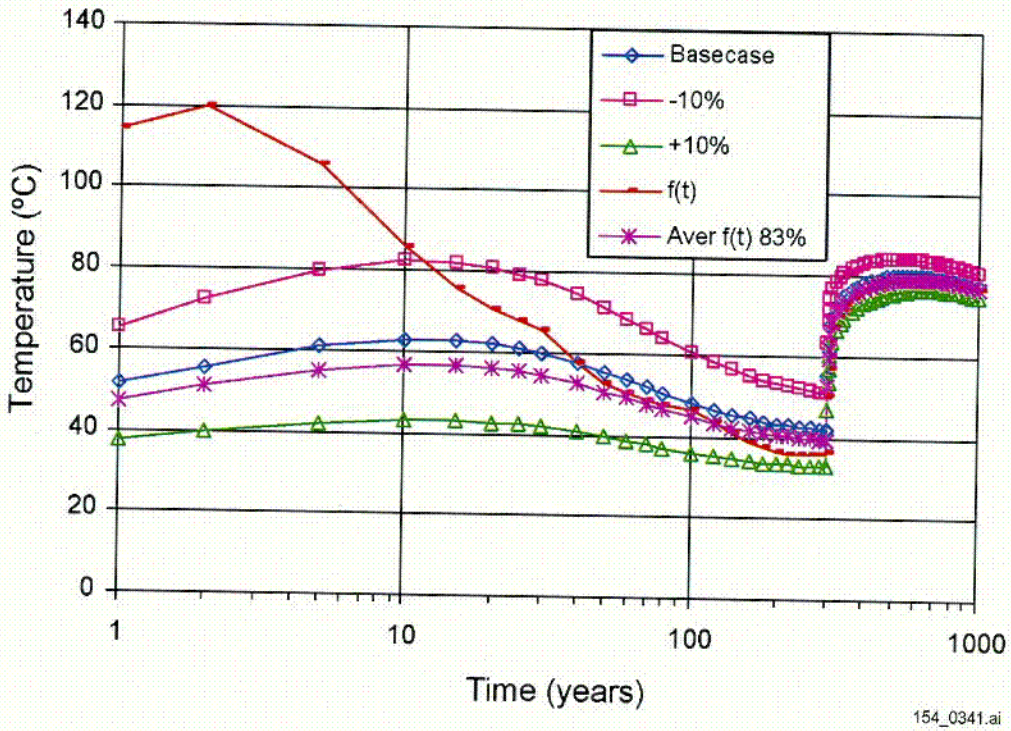

154_0341.ai

Source: Produced using files from Leem 2001 [DIRS 154996].

NOTE: Temperature histories presented as a function of ventilation efficiency.

Figure 5.3.2.4.2-9. Drip Shield Top Temperature Histories for the Lower-Temperature Operating Mode

C04

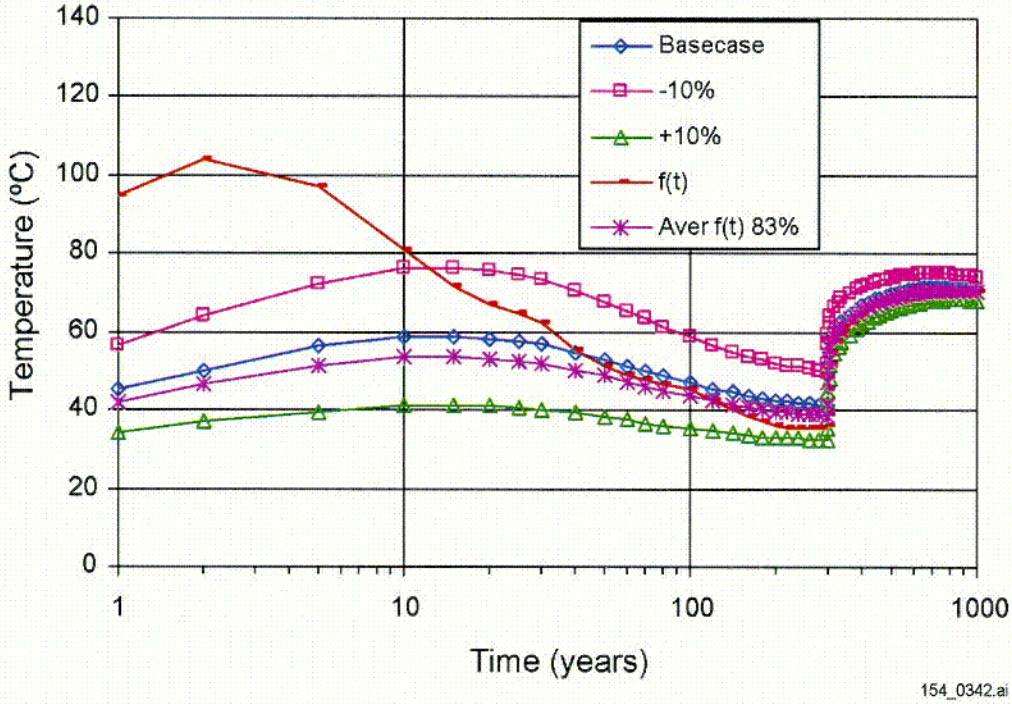

154_0342.ai

Source: Produced using files from Leem 2001 [DIRS 154996].

NOTE: Temperature histories presented as a function of ventilation efficiency.

Figure 5.3.2.4.2-10. Drift Wall Crown Temperature Histories for the Lower-Temperature Operating Mode

C05

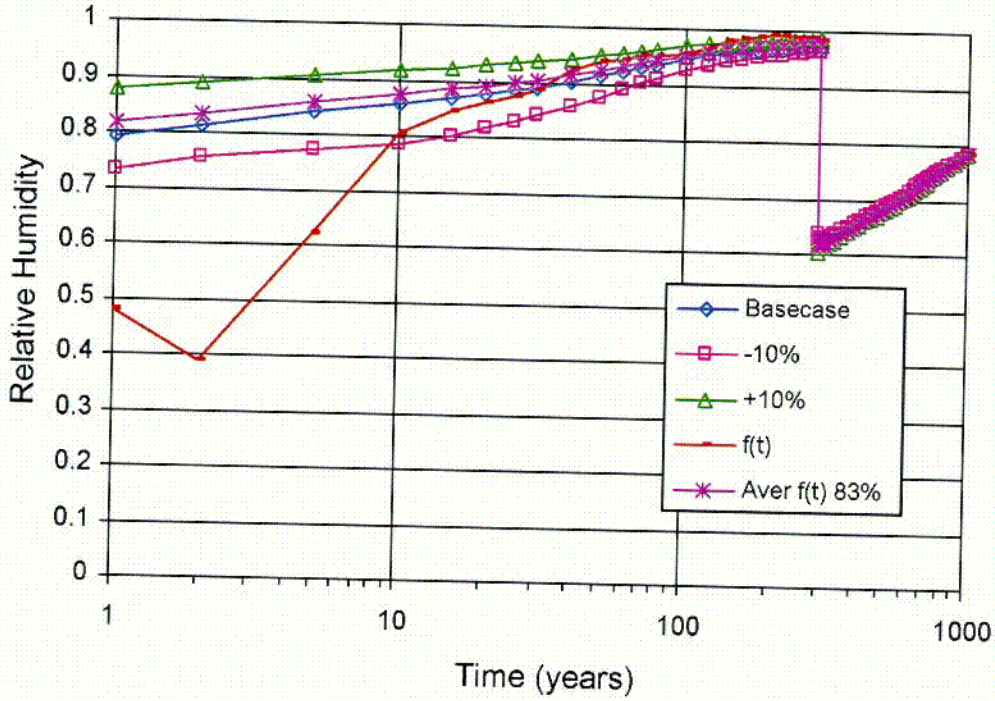

154_0343.ai

Source: Produced using files from Leem 2001 [DIRS 154996].

NOTE: Relative humidity histories presented as a function of ventilation efficiency.

Figure 5.3.2.4.2-11. Drip Shield Crown Relative Humidity Histories for the Lower-Temperature Operating Mode

C06

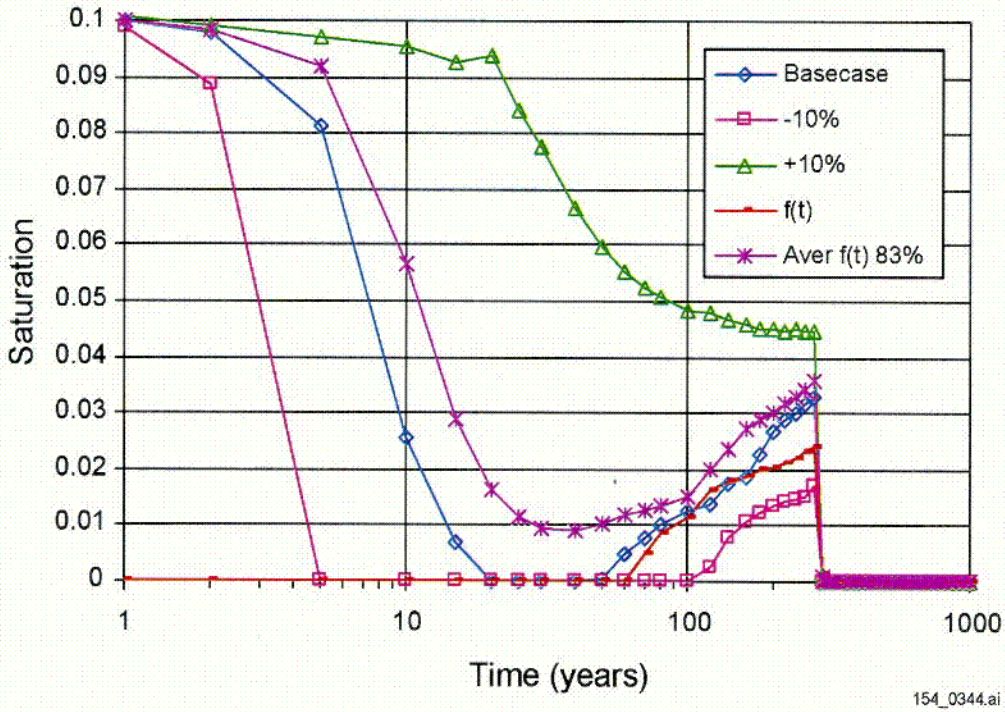

154_0344.ai

Source: Produced using files from Leem 2001 [DIRS 154996].

NOTE: Saturation histories presented as a function of ventilation efficiency.

Figure 5.3.2.4.2-12. Invert (Lower Center) Saturation Histories for the Lower-Temperature Operating Mode

C07

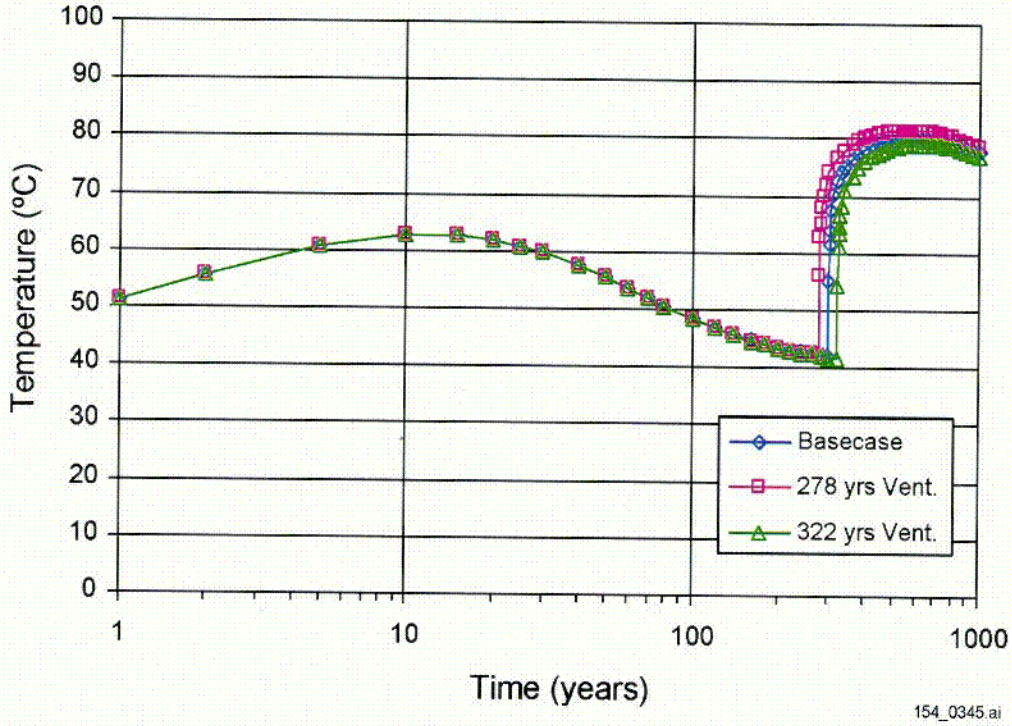

154_0345.ai

Source: Produced using files from Leem 2001 [DIRS 154996].

NOTE: Temperature histories presented as a function of ventilation duration.

Figure 5.3.2.4.3-1. Temperature Histories at the Top of the Drip Shield for the Lower-Temperature Operating Mode

C08

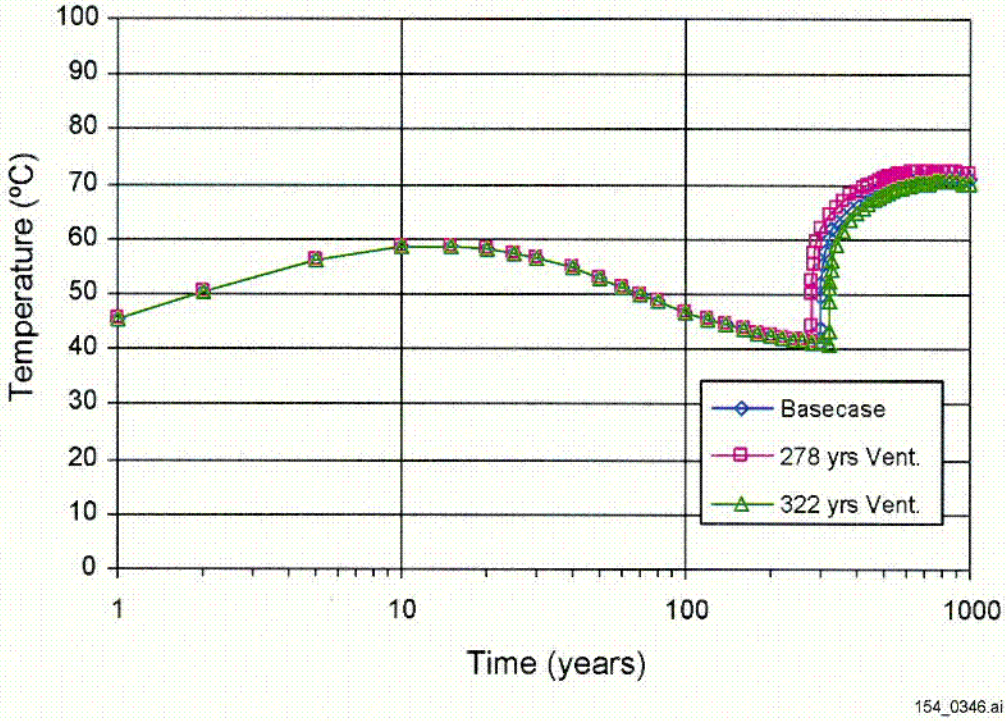

154_0346.ai

Source: Produced using files from Leem 2001 [DIRS 154996].

NOTE: Temperature histories presented as a function of ventilation duration.

Figure 5.3.2.4.3-2. Temperature Histories at the Drift Wall Crown for the Lower-Temperature Operating Mode

C09

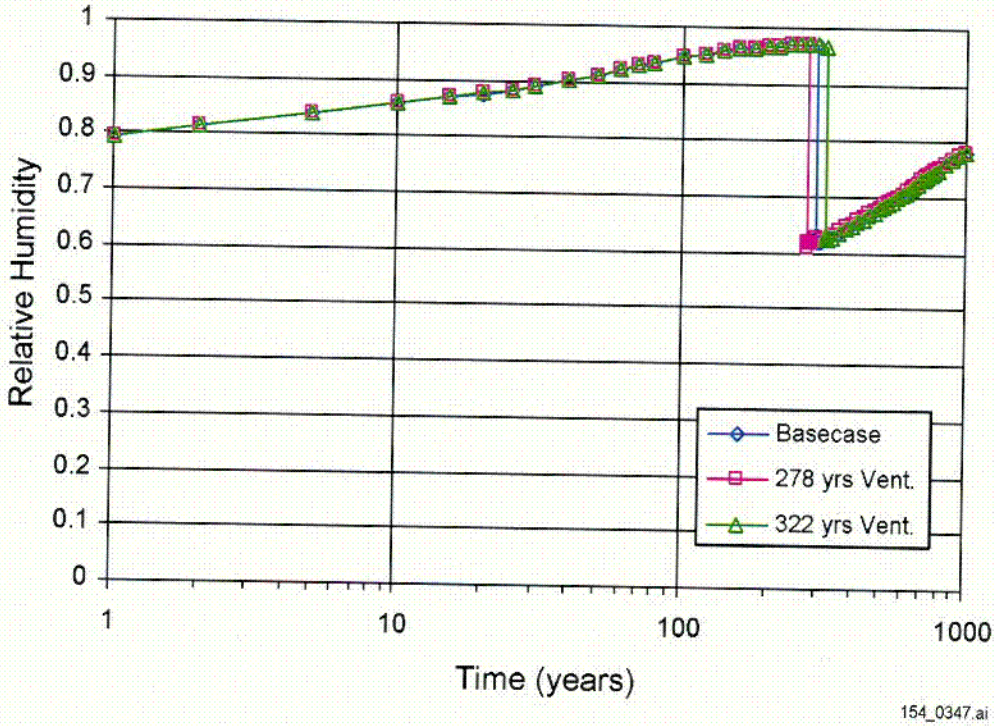

154_0347.ai

Source: Produced using files from Leem 2001 [DIRS 154996].

NOTE: Relative humidity histories presented as a function of ventilation duration.

Figure 5.3.2.4.3-3. Relative Humidity Histories at the Top of the Drip Shield for the Lower-Temperature Operating Mode

C10

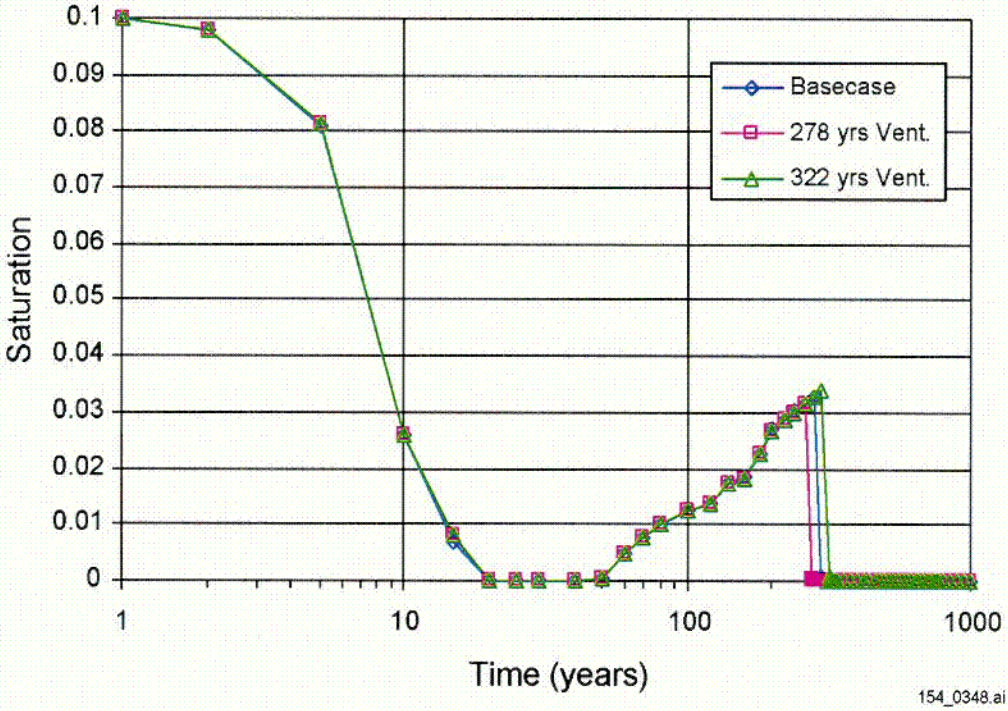

154_0348.ai

Source: Produced using files from Leem 2001 [DIRS 154996].

NOTE: Saturation histories presented as a function of ventilation duration.

Figure 5.3.2.4.3-4. Saturation Histories at the Lower-Center of the Invert for the Lower-Temperature Operating Mode

C11

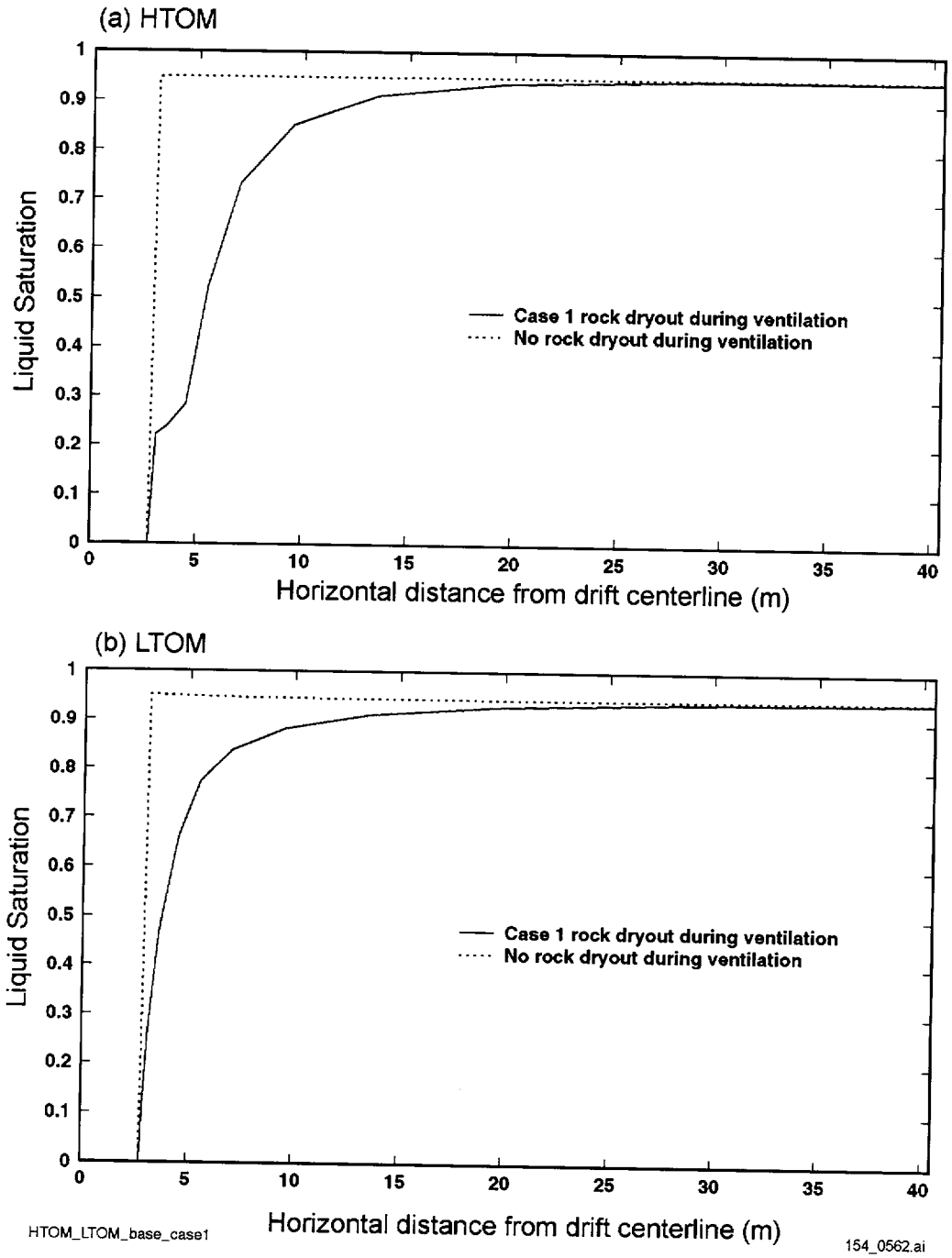

154_0562.ai

Source: Buscheck 2001 [DIRS 155012].

NOTE: The liquid saturations pertain to the matrix continuum.

Figure 5.3.2.4.4-1. Lateral Extent of Host-Rock Dryout Due to Ventilation for Case 1 for the Higher- and Lower-Temperature Operating Modes

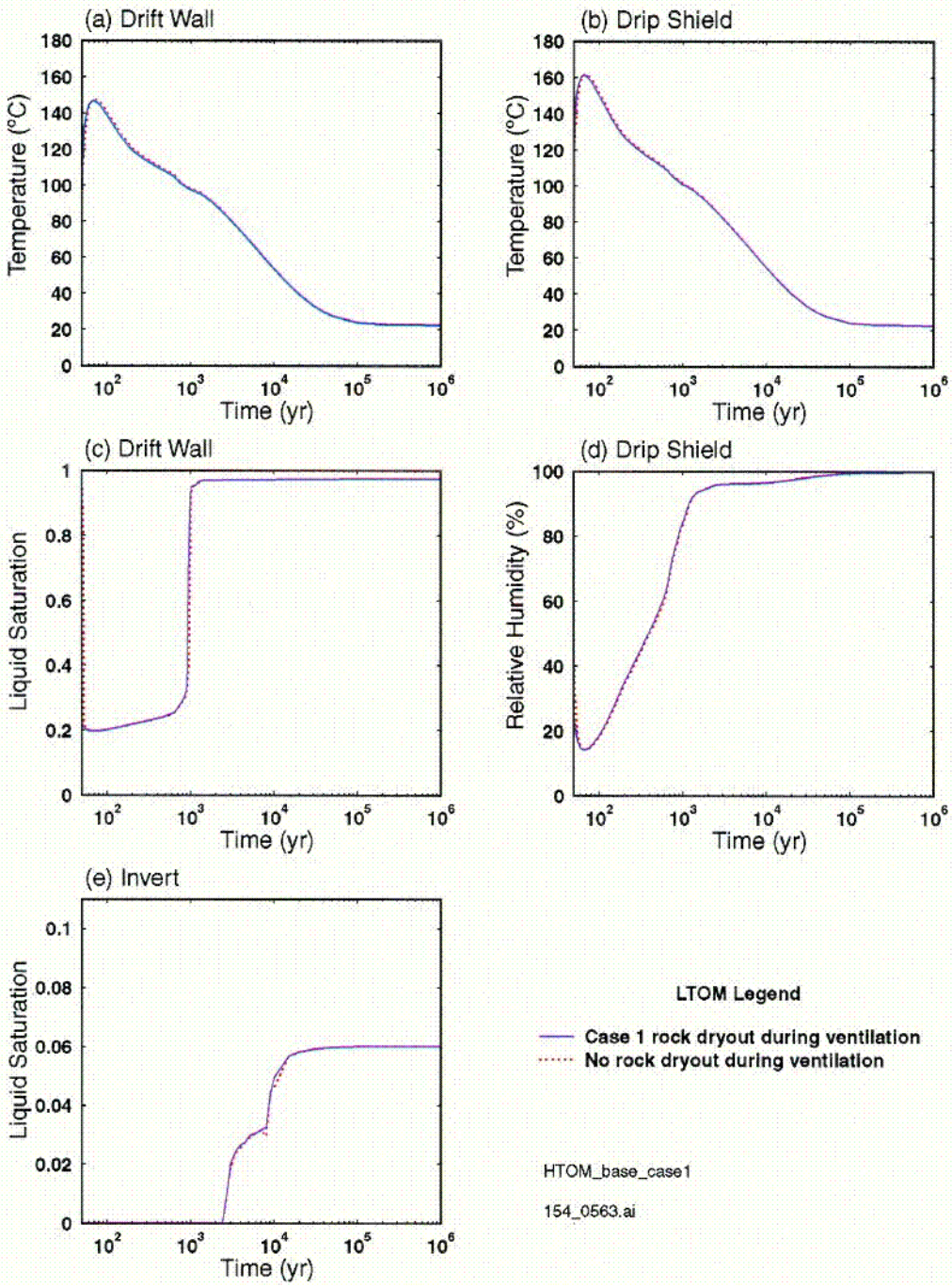

154_0563.ai

Source: Buscheck 2001 [DIRS 155012].

NOTE: The results for the base-case LDTH submodel that neglects the influence of preclosure dryout are also given. The drift wall liquid saturation pertains to the matrix continuum.

Figure 5.3.2.4.4-2. Temperature of the Drift Wall and the Drip Shield, Relative Humidity on the Drip Shield, and Liquid Saturation at the Drift Wall and in the Invert for Case 1 of the Higher-Temperature-Operating Mode

C12

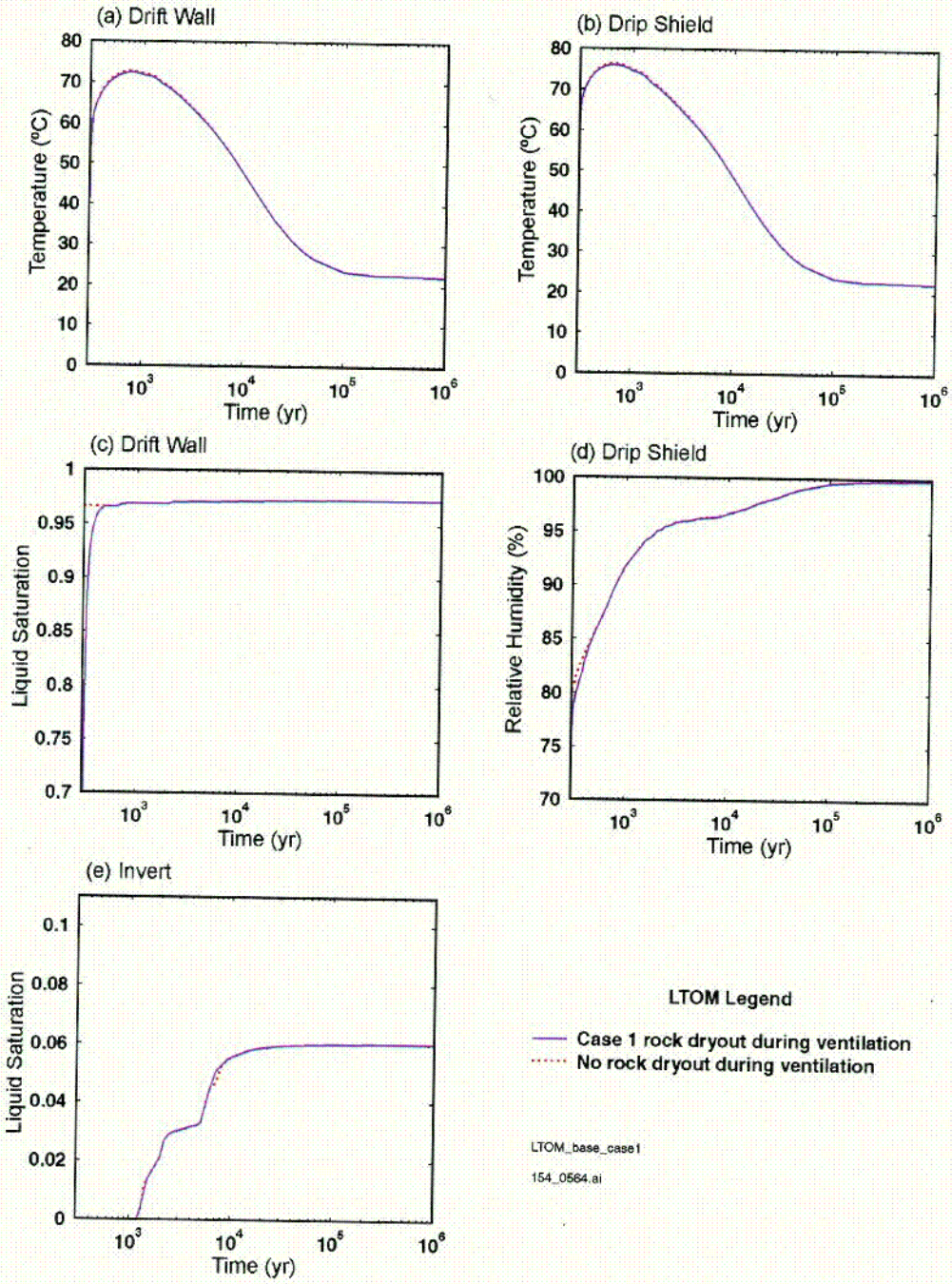

154_0564.ai

Source: Buscheck 2001 [DIRS 155012].

NOTE: The results for the base-case LDTH submodel that neglects the influence of preclosure dryout are also given. The drift wall liquid saturation pertains to the matrix continuum.

Figure 5.3.2.4.4-3. Temperature of the Drift Wall and the Drip Shield, Relative Humidity on the Drip Shield, and Liquid Saturation at the Drift Wall and in the Invert for Case 1 of the Lower-Temperature-Operating Mode

C13

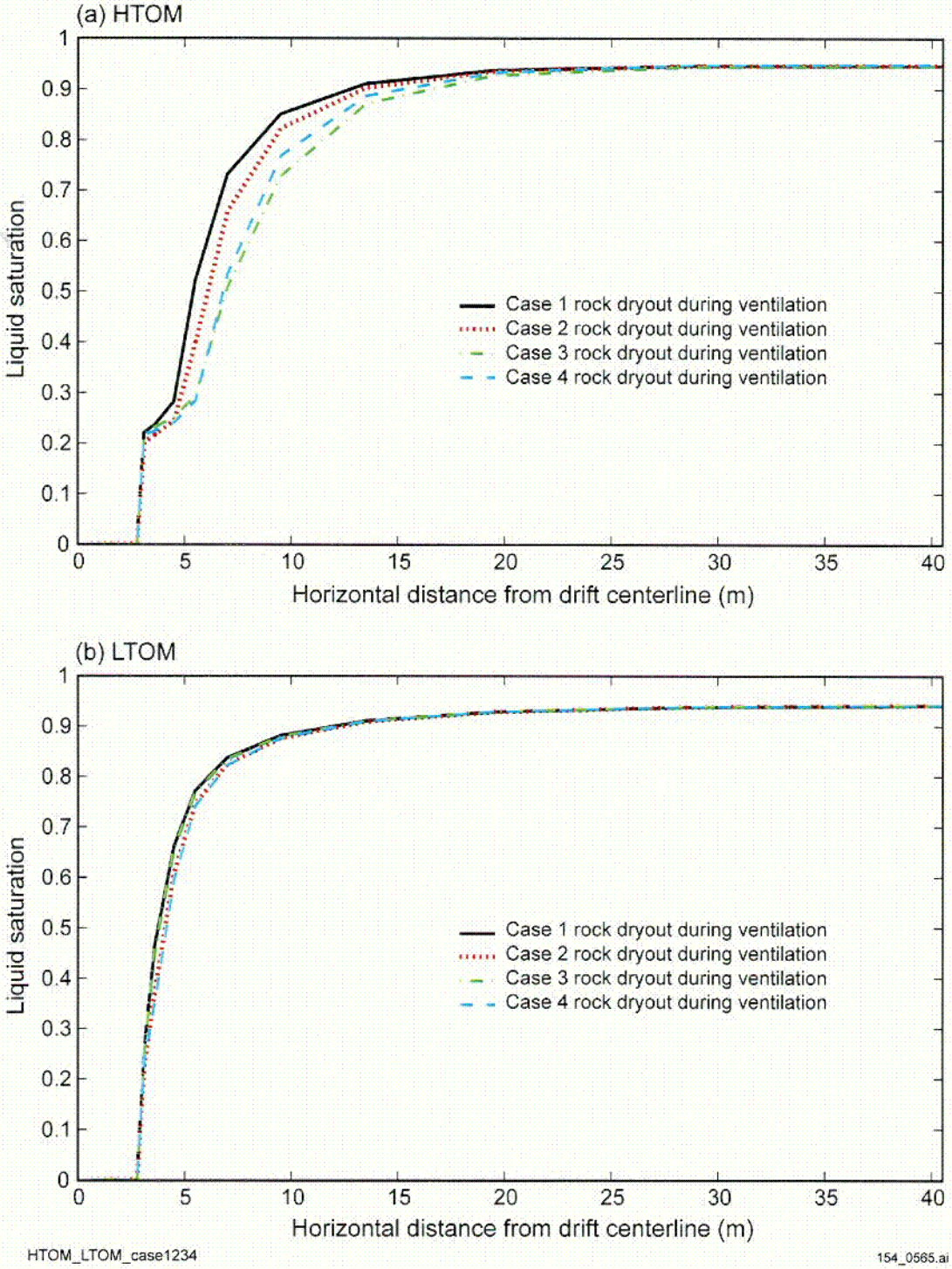

154_0565.ai

Source: Buscheck 2001 [DIRS 155012].

NOTE: The liquid saturations pertain to the matrix continuum.

Figure 5.3.2.4.4-4. Lateral Extent of Host-rock Dryout Due to Ventilation for Cases 1, 2, 3, and 4 for the Higher- and Lower-Temperature Operating Modes

C14

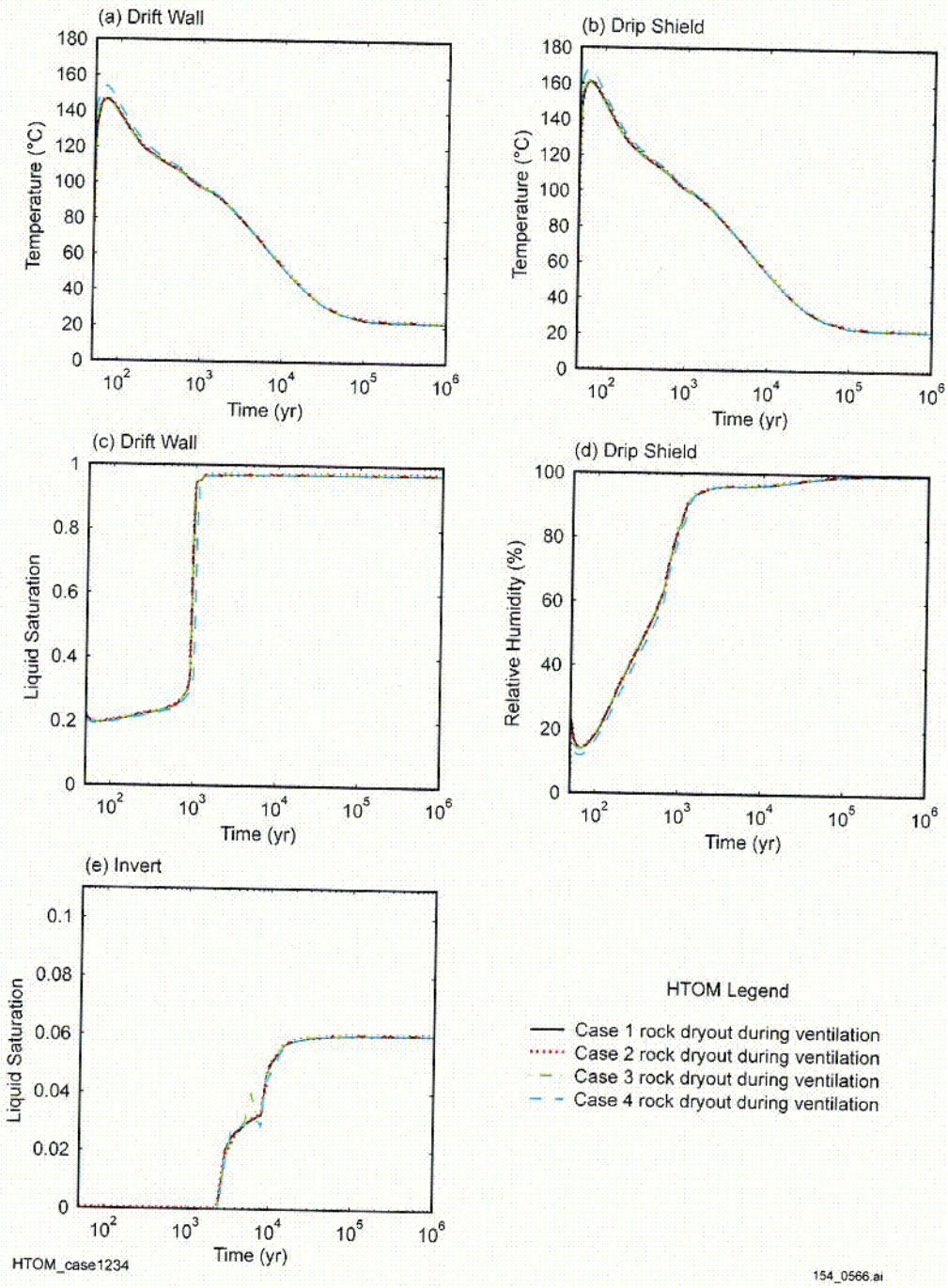

154_0566.ai

Source: Buscheck 2001 [DIRS 155012].

NOTE: The drift wall liquid saturation pertains to the matrix continuum.

Figure 5.3.2.4.4-5. Temperature of the Drift Wall and the Drip Shield, Relative Humidity on the Drip shield, and Liquid Saturation at the Drift Wall and in the Invert for Cases 1, 2, 3, and 4 of the Higher-Temperature Operating Mode

C15

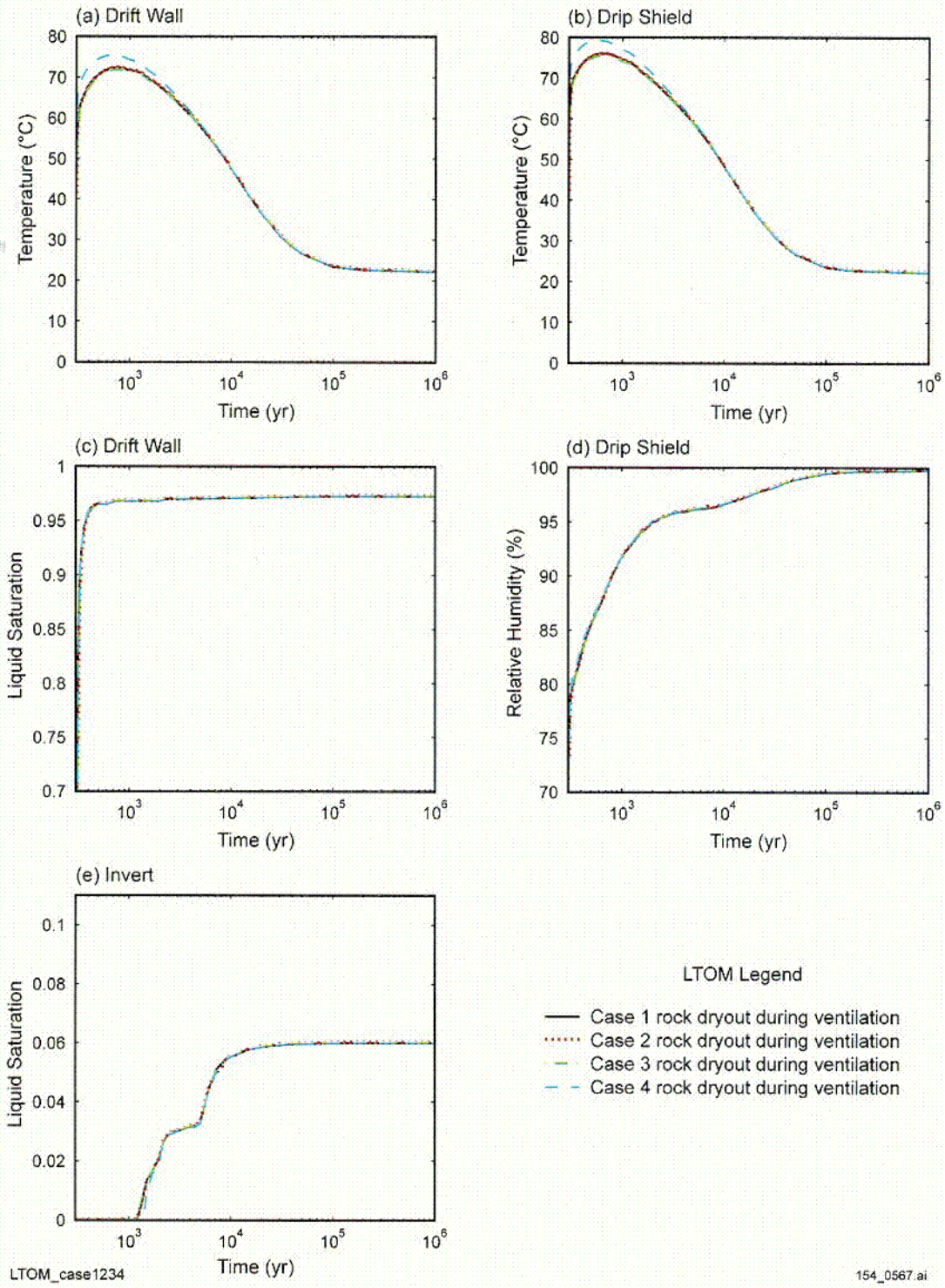

154_0567.ai

Source: Buscheck 2001 [DIRS 155012].

NOTE: The drift wall liquid saturation pertains to the matrix continuum.

Figure 5.3.2.4.4-6. Temperature of the Drift Wall and the Drip Shield, Relative Humidity on the Drip Shield, and Liquid Saturation at the Drift Wall and in the Invert for Cases 1, 2, 3, and 4 of the Lower-Temperature Operating Mode

C16

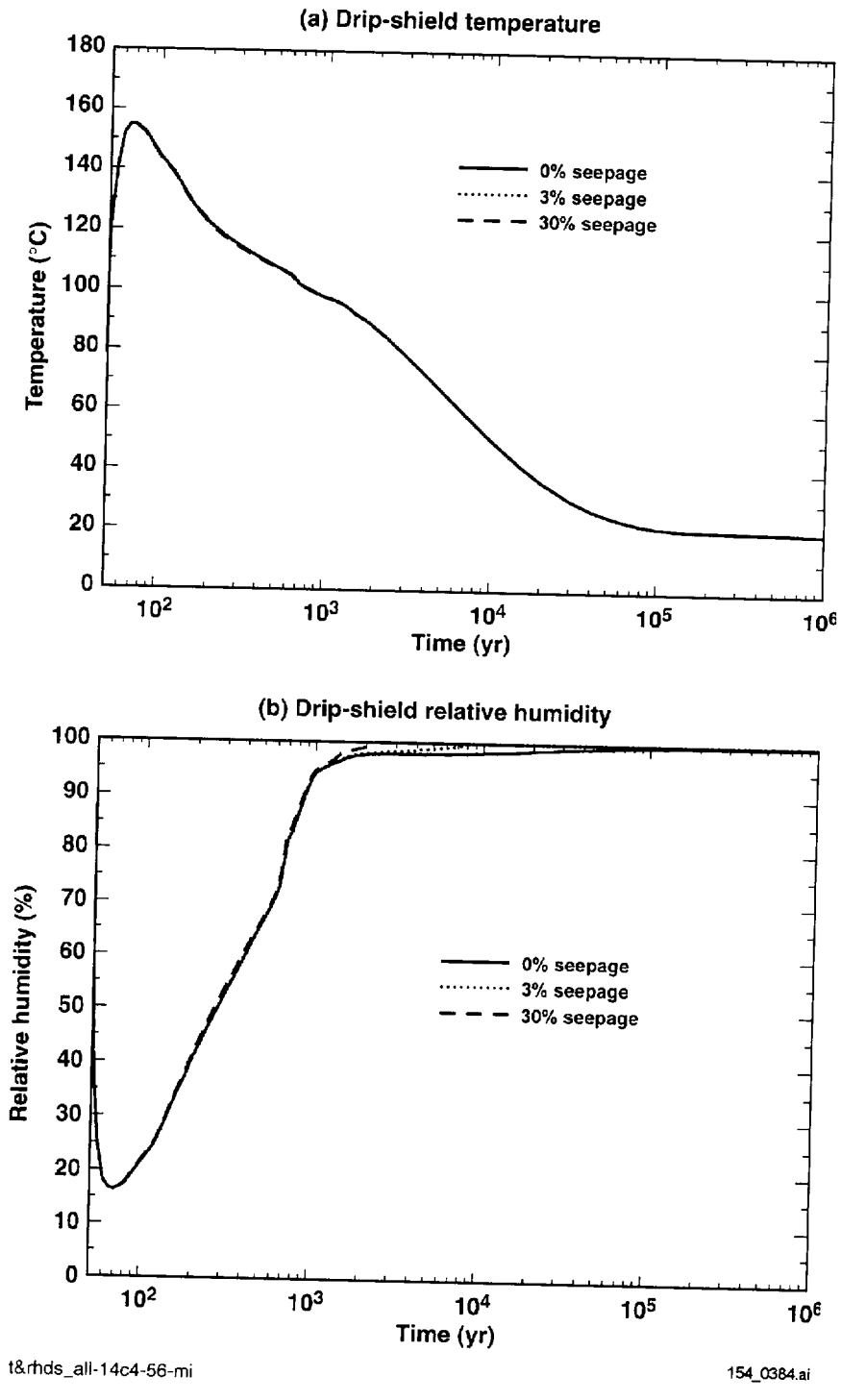

Source: Produced using files from Buscheck 2001 [DIRS 155012], Figure 6-34.

Figure 5.3.2.4.4-7. Temperature (a) and Relative Humidity (b) Histories at the Drip Shield for 0 Percent, 3 Percent, and 30 Percent of the Percolation Flux Seeping into the Drift

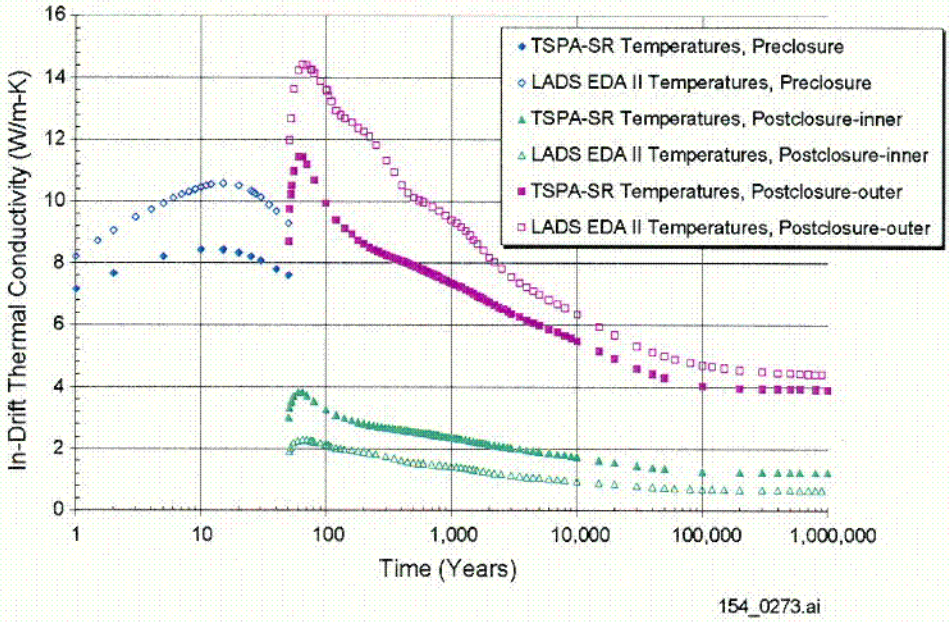

154_0273.ai

Source: Produced using files from Francis 2001 [DIRS 155075].

NOTE: Comparison of the license application design selection (LADS) design and TSPA-SR Rev 00 effective thermal conductivities (postclosure inner is between the waste package and drip shield, postclosure outer is between the drip shield and drift wall).

Figure 5.3.2.4.5-1. Comparison of Thermal Conductivities

C17

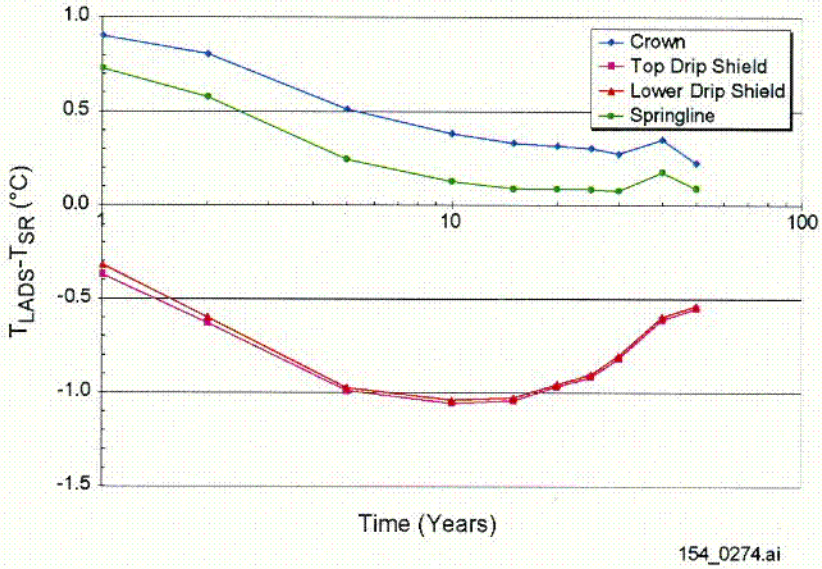

154_0274.ai

Source: Produced using files from Francis 2001 [DIRS 155075].

NOTE: Comparison of preclosure temperature differences at a number of in-drift locations due to effective thermal conductivities developed from two repository designs.

Figure 5.3.2.4.5-2. Comparison of Preclosure Temperature Differences at In-Drift Locations

C18

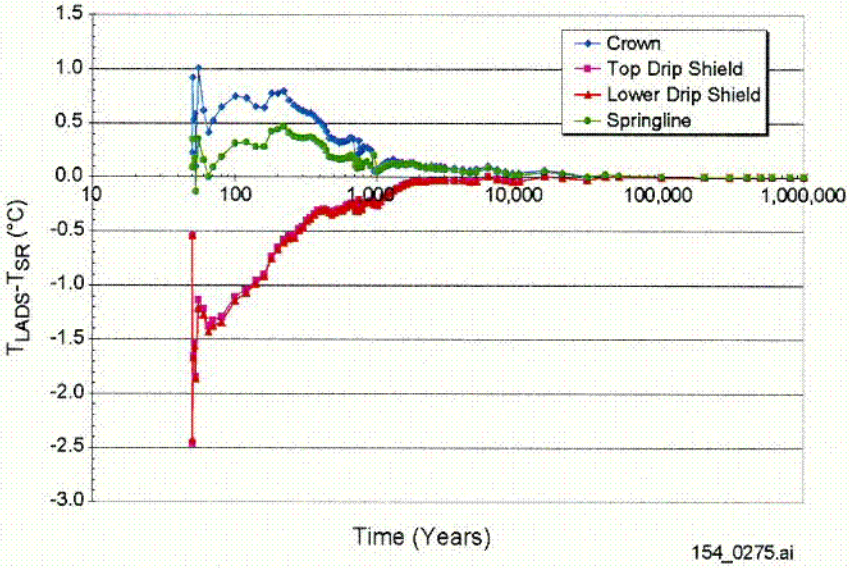

154_0275.ai

Source: Produced using files from Francis 2001 [DIRS 155075].

NOTE: Comparison of postclosure temperature differences at a number of in-drift locations due to effective thermal conductivities developed from two repository designs.

Figure 5.3.2.4.5-3. Comparison of Postclosure Temperature Differences at In-Drift Locations

C19

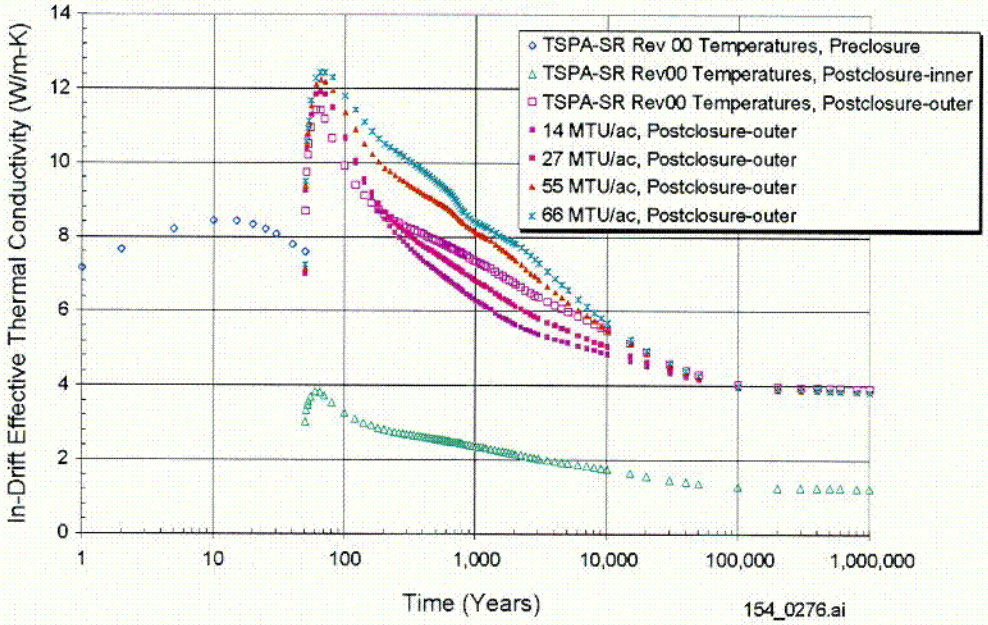

154_0276.ai

Source: Produced using files from Francis 2001 [DIRS 155075].

Figure 5.3.2.4.5-4. Comparison of the Effective Thermal Conductivities Developed Using the TSPA-SR Rev 00 Design and Using Four Areal Mass Loadings

C20

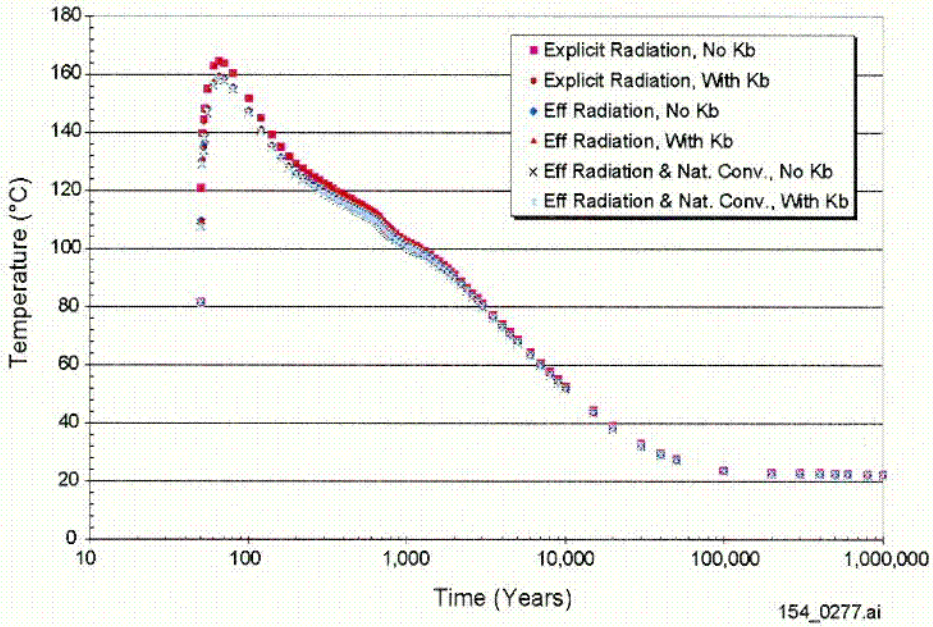

154_0277.ai

Source: Produced using files from Francis 2001 [DIRS 155075].

Figure 5.3.2.4.5-5. Temperature at the Drip Shield for Explicit and Approximated Thermal Radiation and Natural Convection

C21

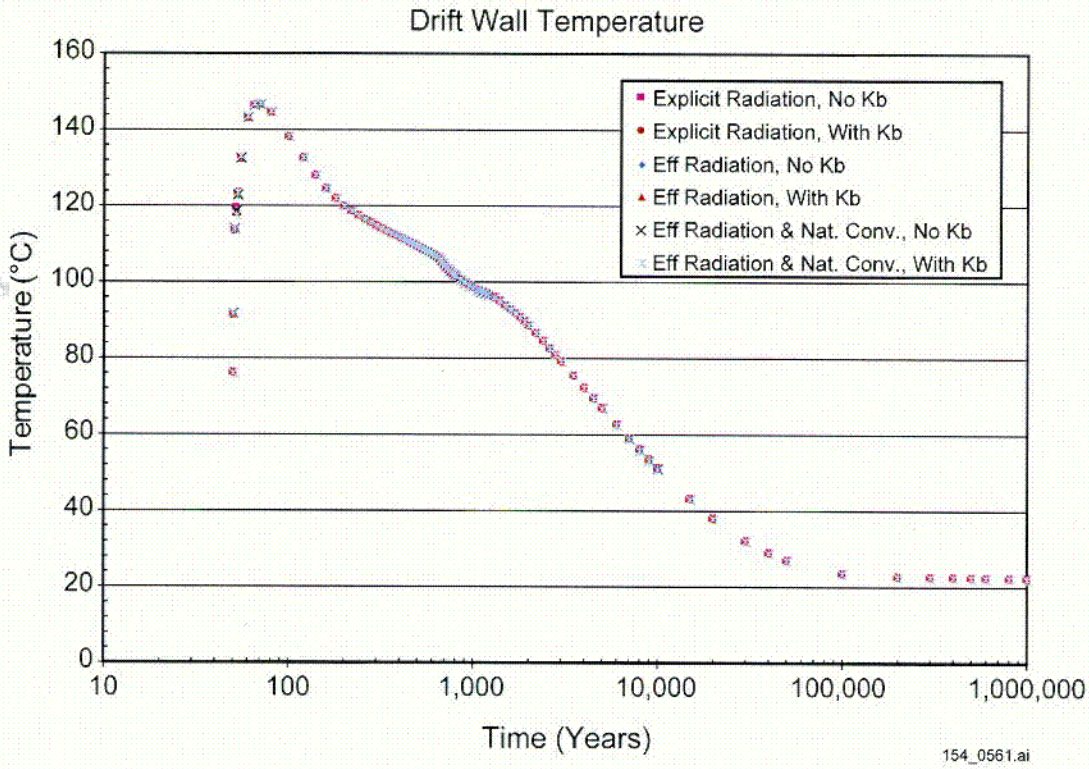

154_0561.ai

Source: Produced using files from Francis 2001 [DIRS 155075].

Figure 5.3.2.4.5-5a. Temperature Comparison at the Drift Wall for Explicit and Approximated Thermal Radiation and Natural Convection

C22

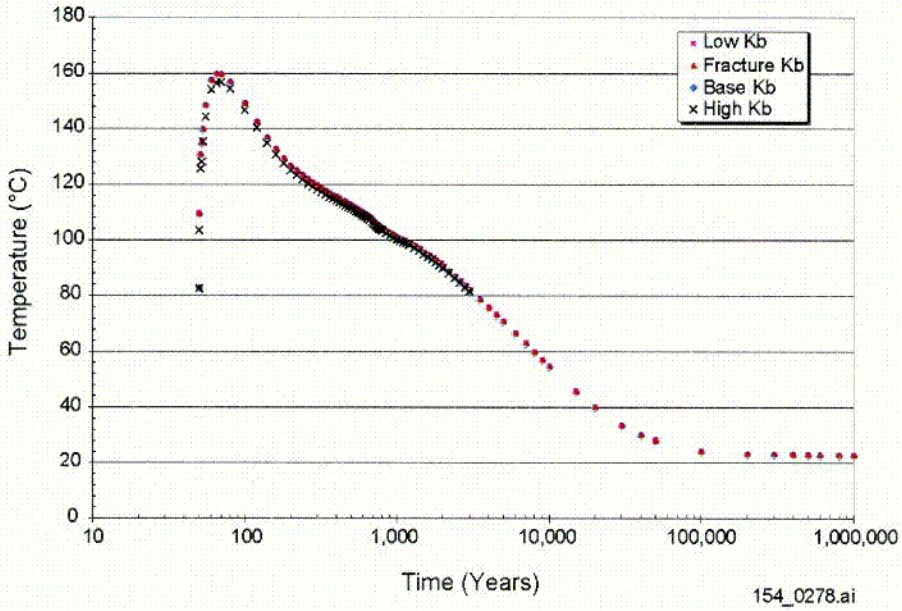

154_0278.ai

Source: Produced using files from Francis 2001 [DIRS 155075].

NOTE: Temperature histories at the base of the drip shield for a range of air permeabilities and the higher-temperature operating mode.

Figure 5.3.2.4.5-6. Temperature Histories at the Base of the Drip Shield

C23

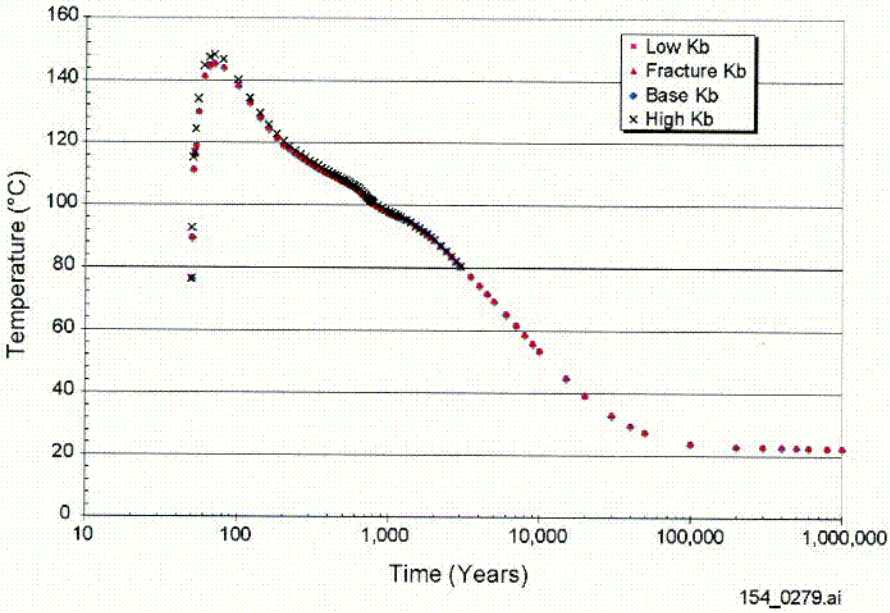

154_0279.ai

Source: Produced using files from Francis 2001 [DIRS 155075].

NOTE: Temperature histories at the crown of the drift wall for a range of air permeabilities, for the higher-temperature operating mode.

Figure 5.3.2.4.5-7. Temperature Histories at the Crown of the Drift Wall

C24

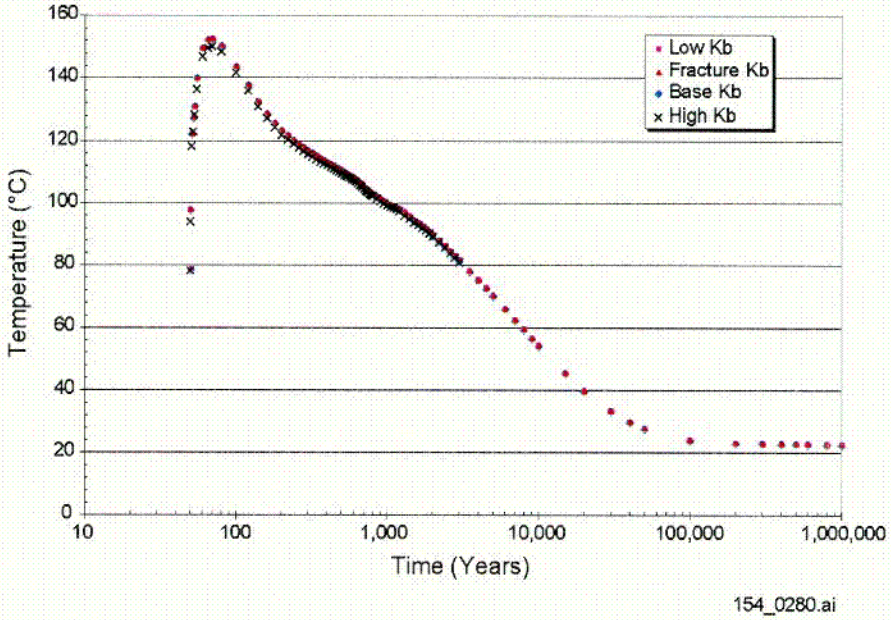

154_0280.ai

Source: Produced using files from Francis 2001 [DIRS 155075].

NOTE: Temperature histories at the bottom-center of the invert for a range of air permeabilities, for the higher-temperature operating mode.

Figure 5.3.2.4.5-8. Temperature Histories at the Bottom-Center of the Invert

C25

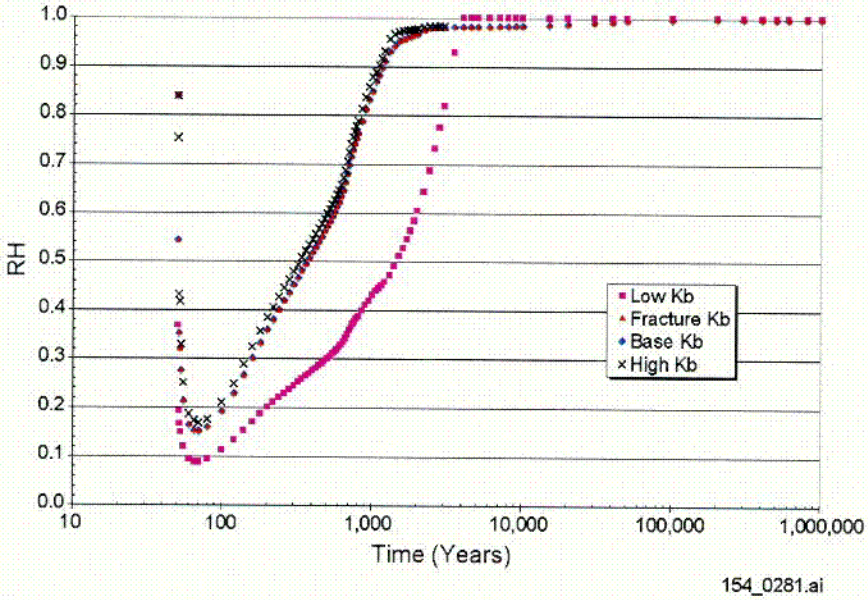

154_0281.ai

Source: Produced using files from Francis 2001 [DIRS 155075].

NOTE: Relative humidity (RH) histories at the base of the drip shield for a range of air permeabilities, for the higher-temperature operating mode.

Figure 5.3.2.4.5-9. Relative Humidity Histories at the Base of the Drip Shield

C26

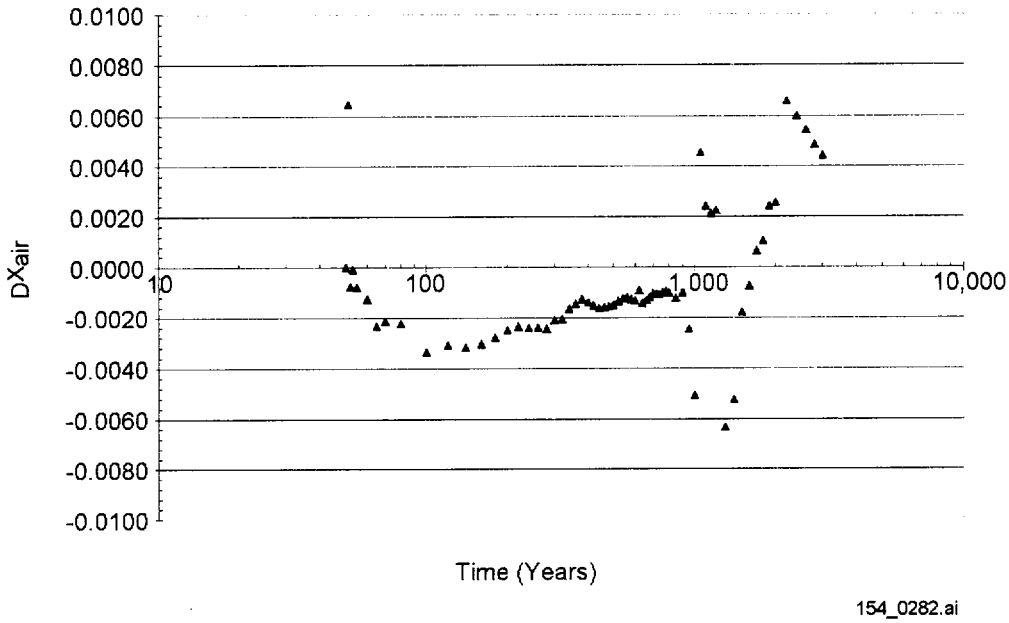

154_0282.ai

Source: Produced using files from Francis 2001 [DIRS 155075].

NOTE: Air mass fraction (D^Xair) differences between the high permeability case and the base case, at the base of the drip shield for the higher-temperature operating mode.

Figure 5.3.2.4.5-10. Air Mass Fraction Differences Between the High Permeability and Base Cases at the Base of the Drip Shield

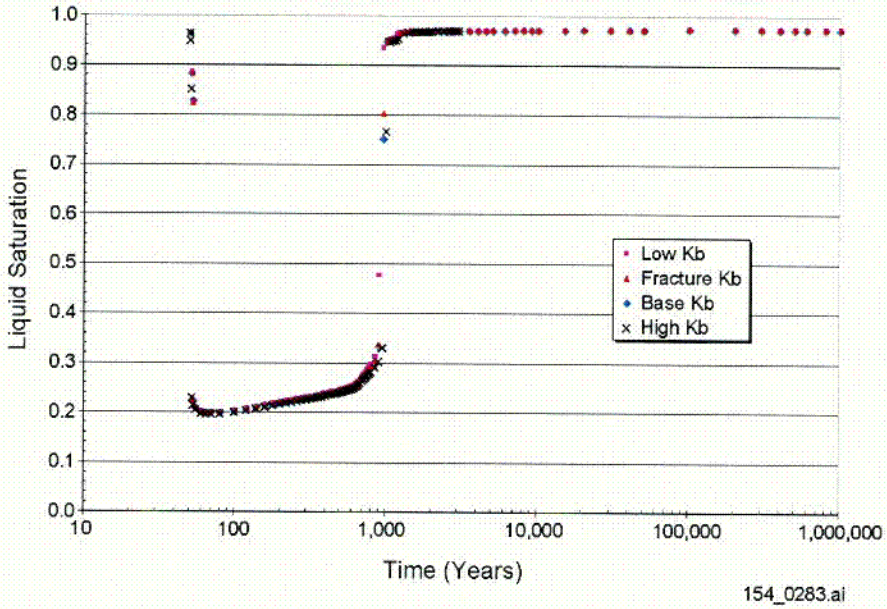

154_0283.ai

Source: Produced using files from Francis 2001 [DIRS 155075].

NOTE: Saturation history of near-field rock at the crown of the drift wall for a range of air permeabilities, for the higher-temperature operating mode.

Figure 5.3.2.4.5-11. Saturation History of Near-Field Rock at the Crown of the Drift Wall

C 27

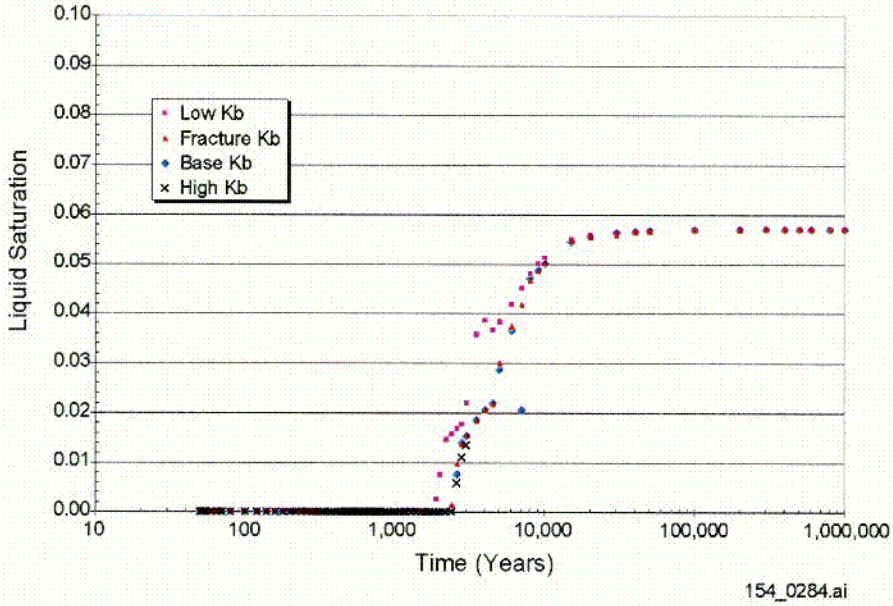

154_0284.ai

Source: Produced using files from Francis 2001 [DIRS 155075].

NOTE: Saturation history of the bottom-center of the invert for a range of air permeabilities, for the higher-temperature operating mode.

Figure 5.3.2.4.5-12. Saturation History of the Bottom-Center of the Invert

C28

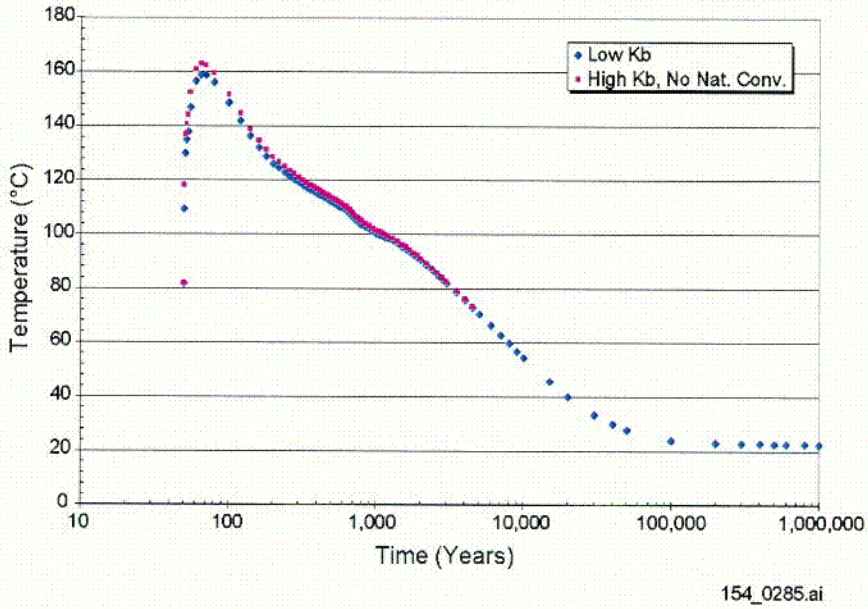

154_0285.ai

Source: Produced using files from Francis 2001 [DIRS 155075].

NOTE: Temperature histories at the top of the drip shield calculated with a porous medium model and with a correlation-based effective thermal conductivity model.

Figure 5.3.2.4.5-13. Temperature Histories at the Top of the Drip Shield

C29

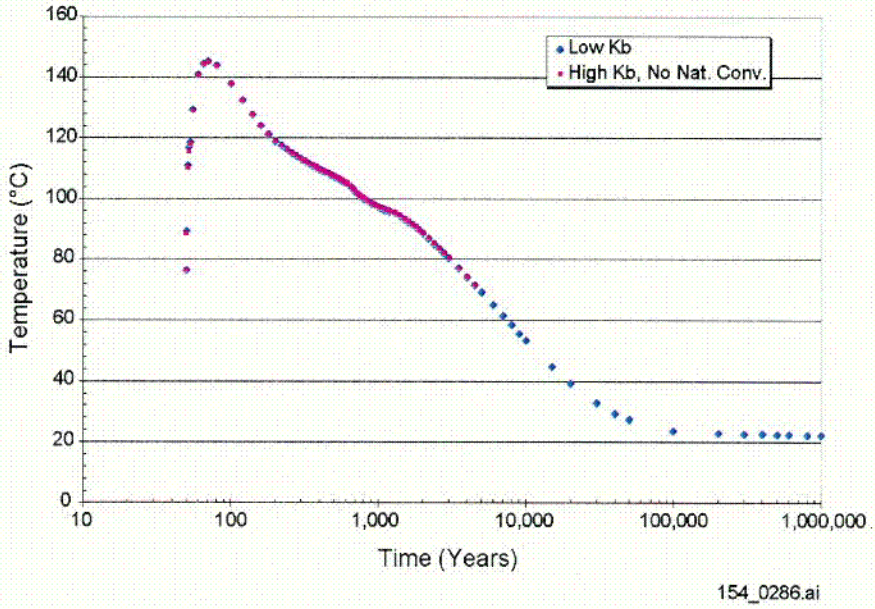

154_0286.ai

Source: Produced using files from Francis 2001 [DIRS 155075].

NOTE: Temperature histories at the crown of the drift wall calculated with a porous medium model and with a correlation-based effective thermal conductivity model.

Figure 5.3.2.4.5-14. Temperature Histories at the Crown of the Drift Wall

C30

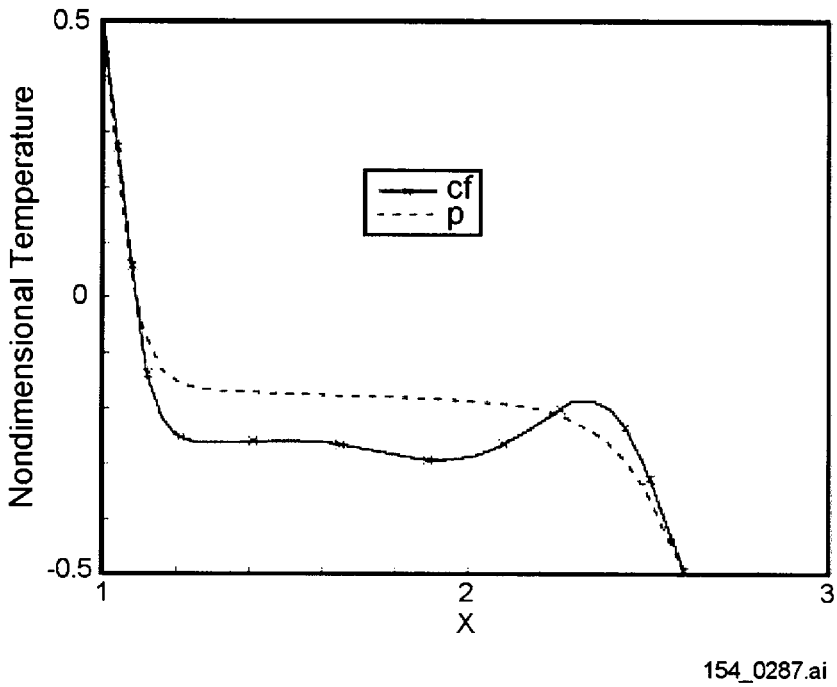

154_0287.ai

Source: Produced using files from Francis 2001 [DIRS 155075].

NOTE: X = horizontal distance; cf= Navier-Stokes CFD model; p= porous medium model.

Figure 5.3.2.4.5-15. Nondimensional Temperature Versus Nondimensional Horizontal Distance for the Horizontal Midplane Through the In-Drift Air

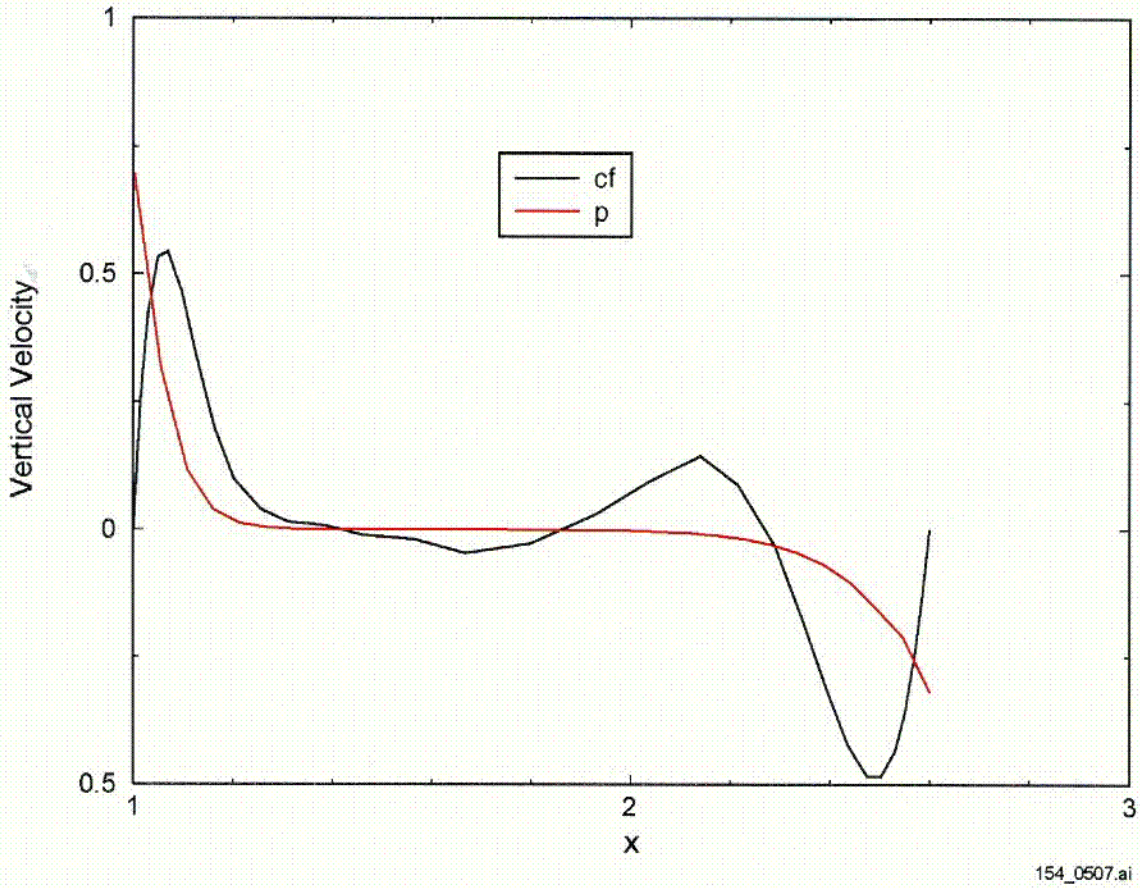

154_0507.ai

Source: Produced using files from Francis 2001 [DIRS 155075].

NOTE: X = horizontal distance. Figure corrected after publication of original source. cf = Navier-Stokes CFD model; p= porous medium model.

Figure 5.3.2.4.5-16. Nondimensional Vertical Velocity Versus Nondimensional Horizontal Distance for the Horizontal Midplane Through the In-Drift Air

C31

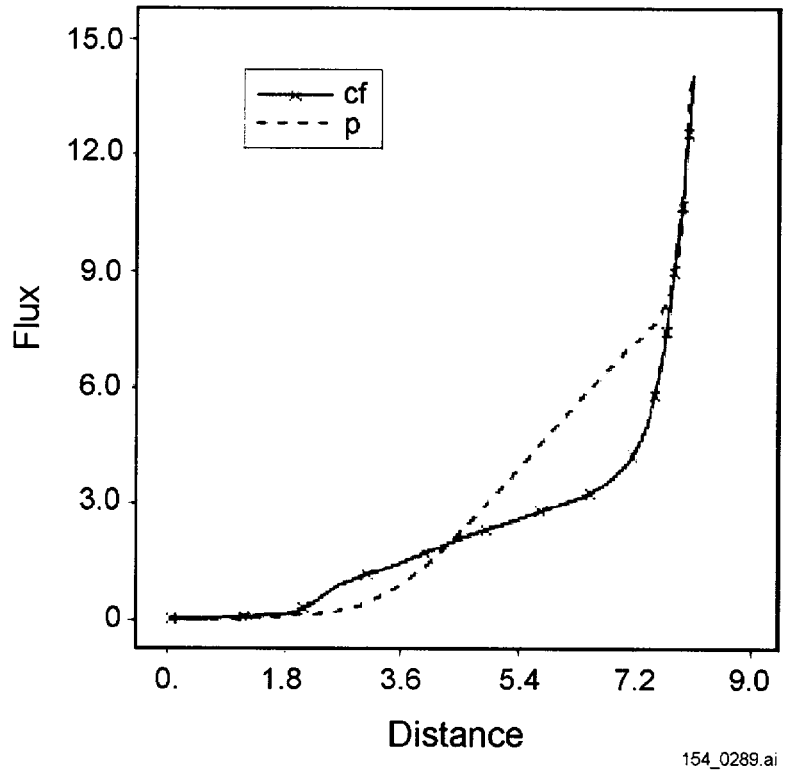

154_0289.ai

Source: Produced using files from Francis 2001 [DIRS 155075].

NOTE: cf= Navier-Stokes CFD model; p= porous medium model.

Figure 5.3.2.4.5-17. Nondimensional Heat Flux on the Cool (Outer) Cylinder Versus Non-Dimensional Distance Along the Cylinder Perimeter

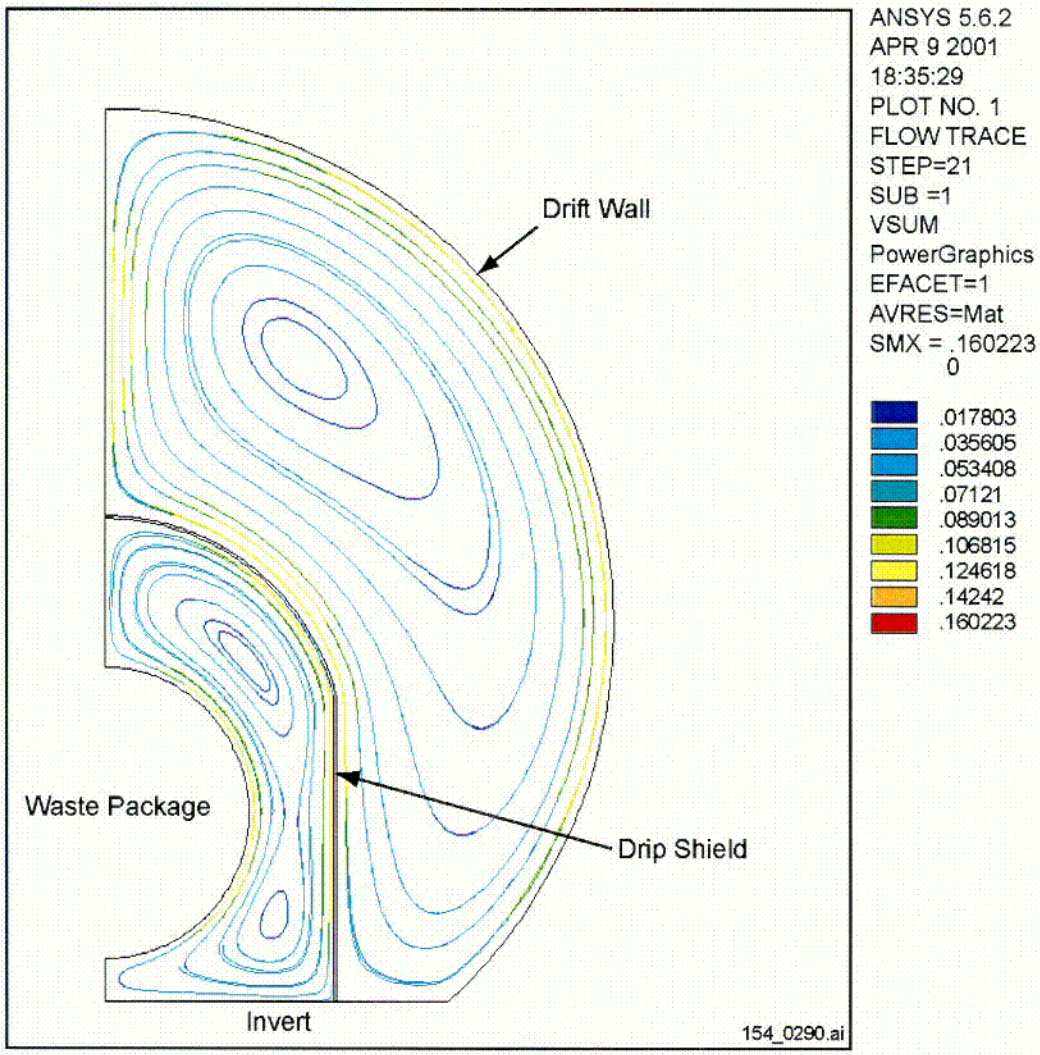

154_0290.ai

Source: Produced using files from Francis 2001 [DIRS 155075].

Figure 5.3.2.4.5-18. Natural Convection Flow Velocities Calculated Using ANSYS

C32

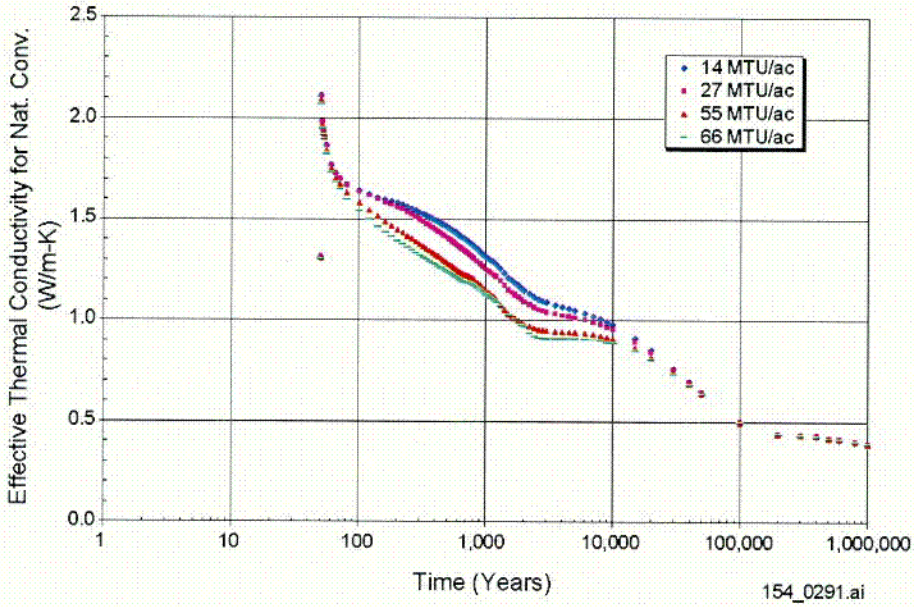

154_0291.ai

Source: Produced using files from Francis 2001 [DIRS 155075].

NOTE: Effective thermal conductivity for natural convection for the higher-temperature operating mode used in the SSPA Volume 2 supplemental analyses (McNeish 2001 [DIRS 155023]).

Figure 5.3.2.4.5-19. Effective Thermal Conductivity for Natural Convection for the Higher-Temperature Operating Mode

C33

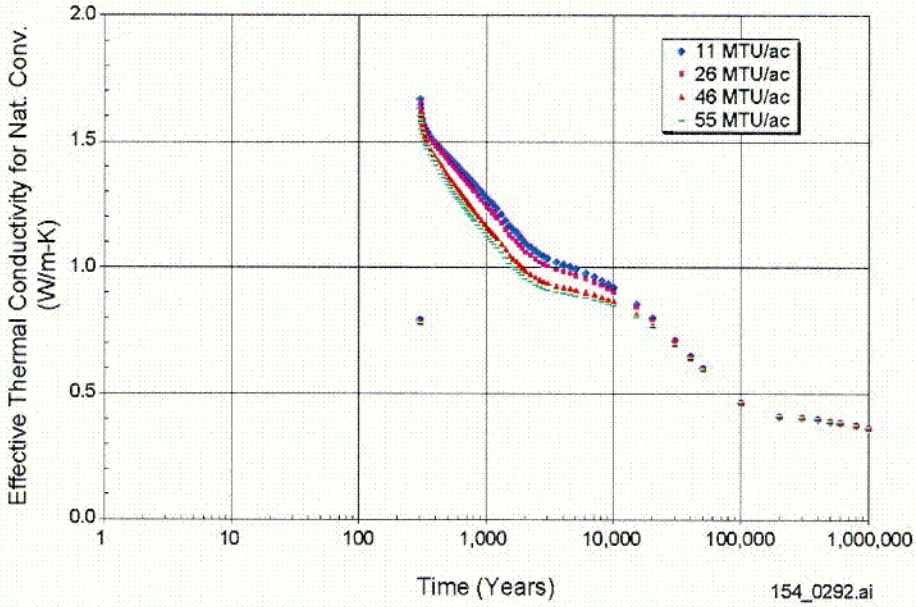

154_0292.ai

Source: Produced using files from Francis 2001 [DIRS 155075].

NOTE: Effective thermal conductivity for natural convection for the lower-temperature operating mode used in SSPA Volume 2 supplemental analyses (McNeish 2001 [DIRS 155023]).

Figure 5.3.2.4.5-20. Effective Thermal Conductivity for Natural Convection for the Lower-Temperature Operating Mode

C34

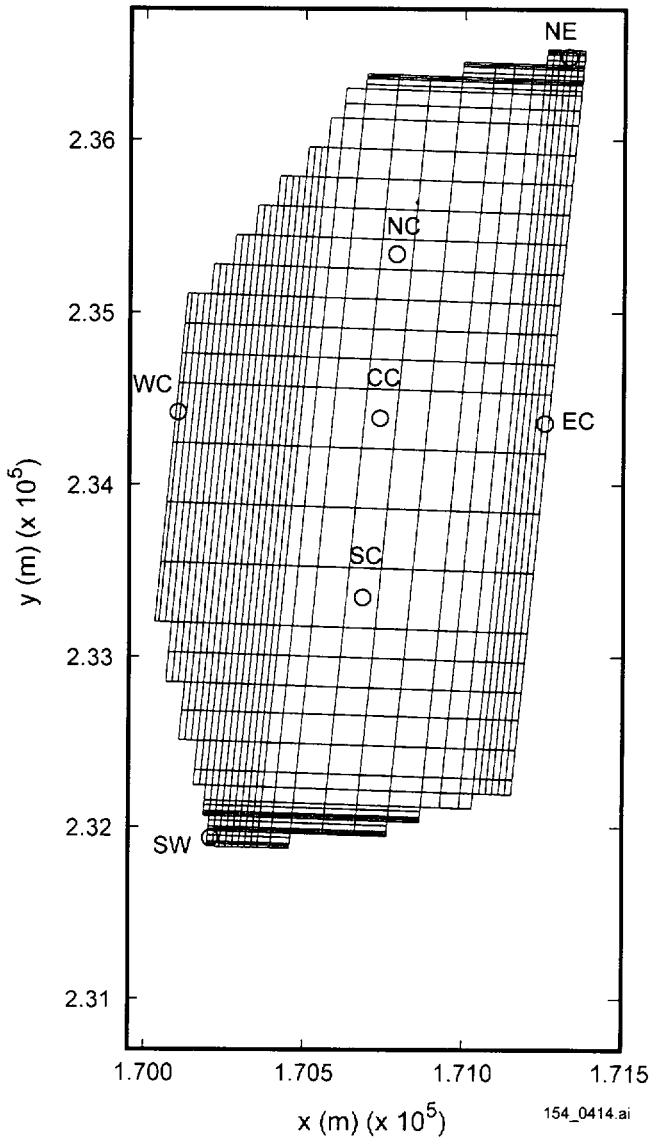

154_0414.ai

Source: Produced using files from Buscheck 2001 [DIRS 155243].

NOTE: Plan view of the potential Higher-Temperature Operating Mode repository showing the geographic locations considered in various analyses. X = east-west distances, Y = north-south distances.

Figure 5.4.1-1. Location of Seven Sites Used in Analyses of the Higher-Temperature Operating Mode Repository

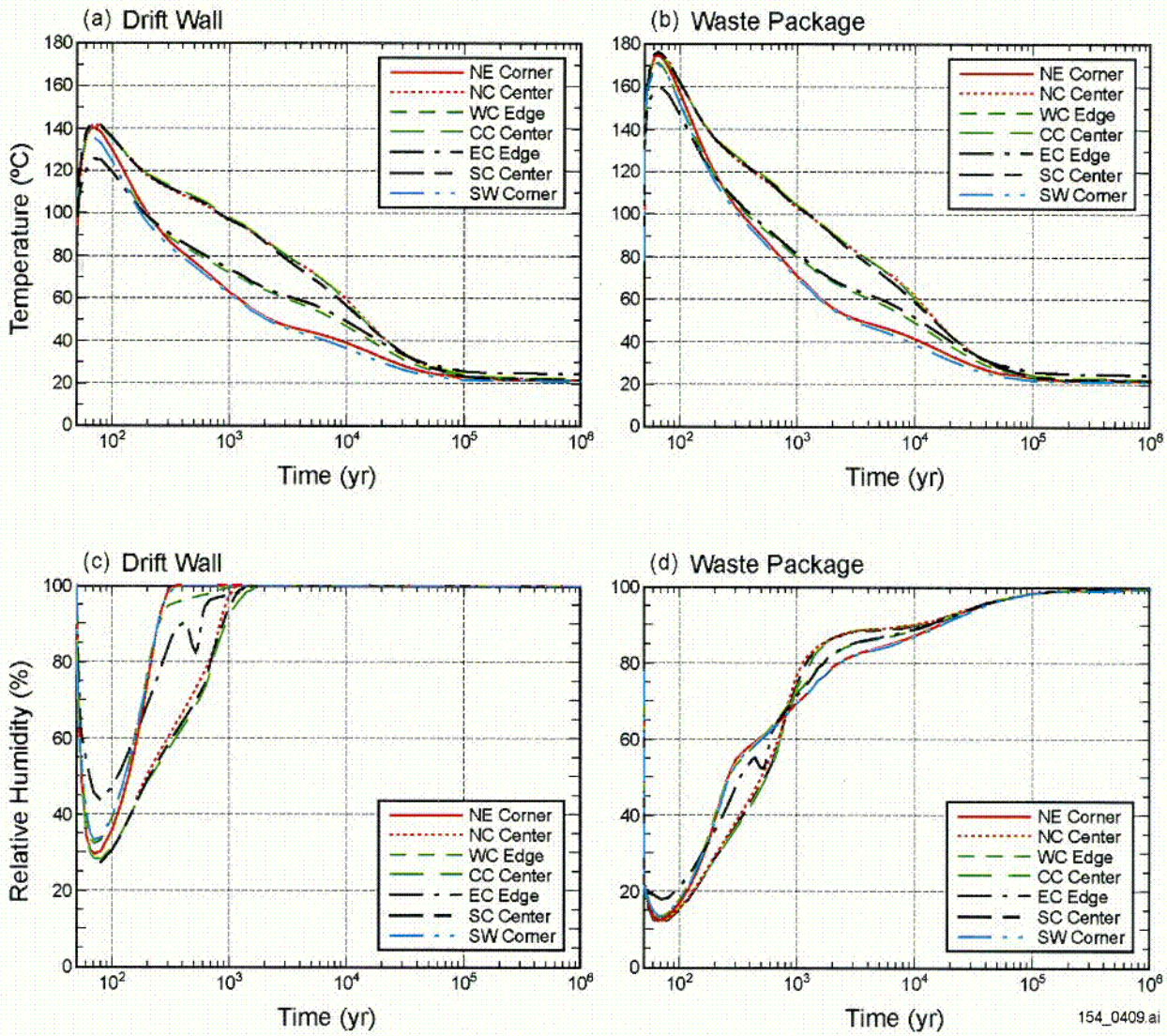

154_0409.ai

Source: Produced using files from Buscheck 2001 [DIRS 155243].

NOTE: Average 21-PWR commercial SNF waste package mean-infiltration flux scenario.

Figure 5.4.1-2. Temperature and Relative Humidity Histories on the Drift Wall and the Waste Package for Seven Locations in the Higher-Temperature Operating Mode Repository

C35

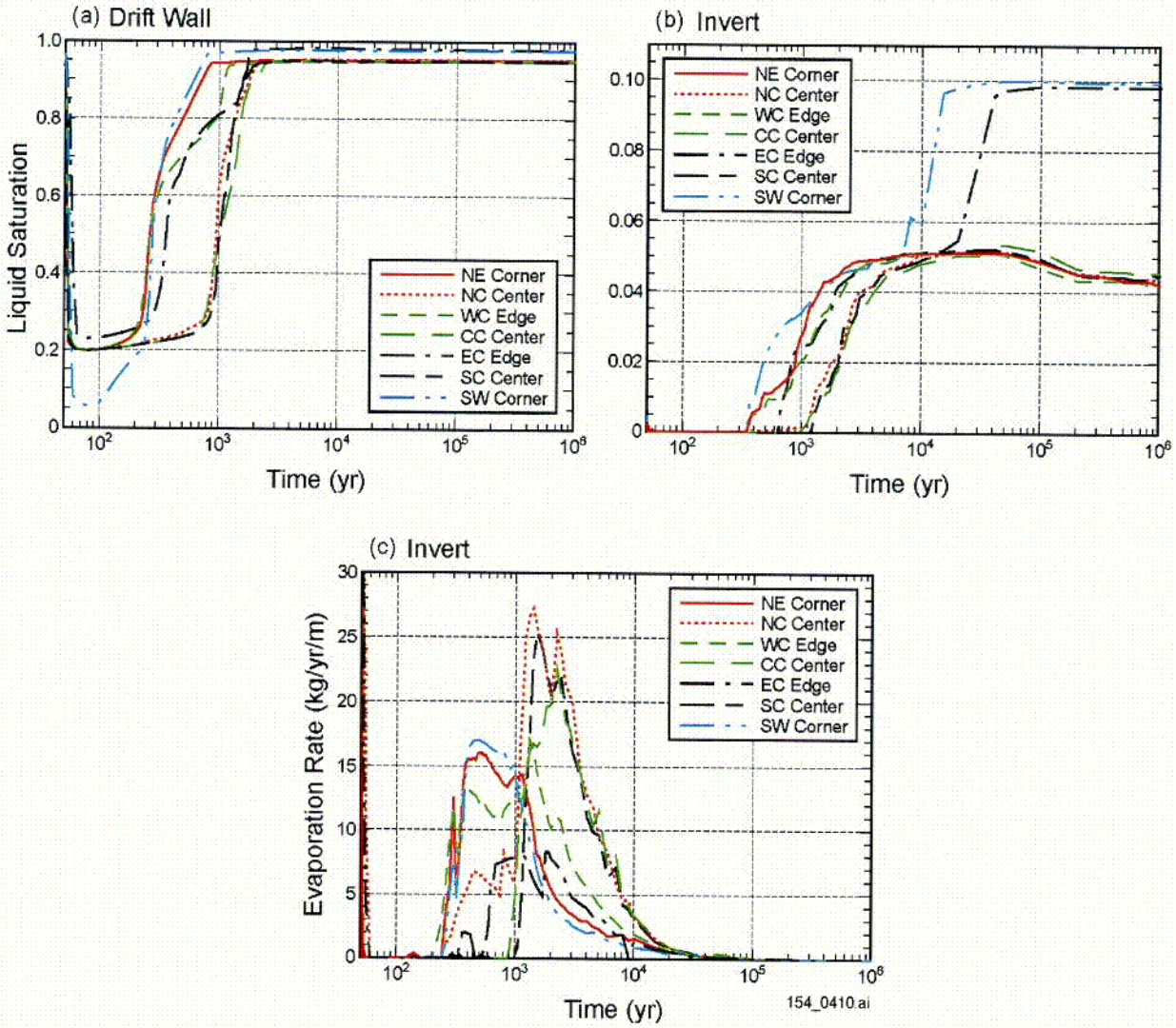

154_0410.ai

Source: Produced using files from Buscheck 2001 [DIRS 155243].

NOTE: Average 21-PWR CSNF waste package Mean-infiltration-flux scenario. Liquid-saturation curves are given for (a) the matrix at the drift wall and for (b) the invert. Evaporation-rate histories are given for the invert (c).

Figure 5.4.1-3. Liquid Saturation and Evaporation Rate Histories for Seven Locations in the Higher-Temperature Operating Mode Repository

C36

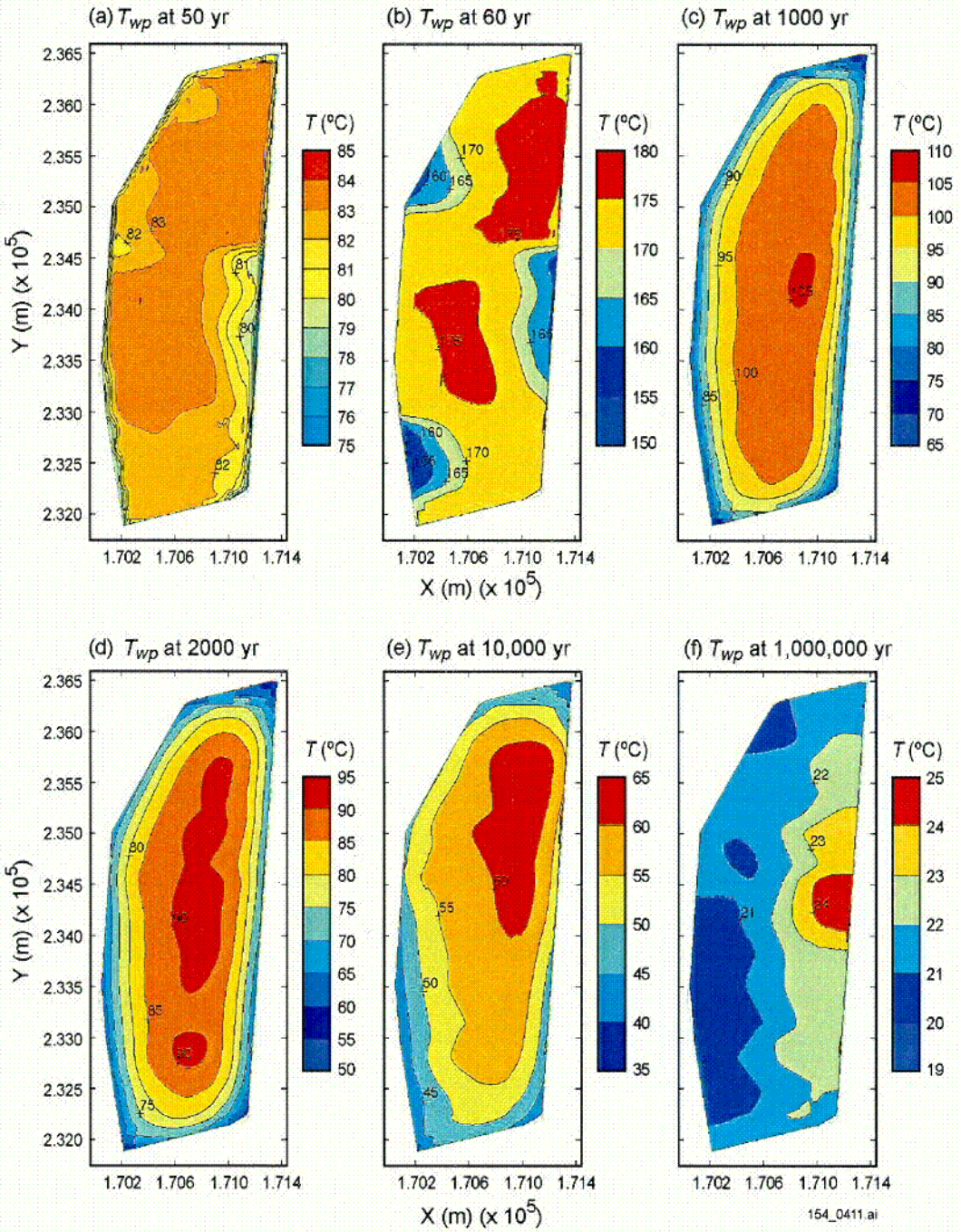

154_0411.ai

Source: Produced using files from Buscheck 2001 [DIRS 155243].

NOTE: Average 21-PWR waste package Mean-infiltration-flux scenario. T_{WP} = waste package temperature, X = east-west distances, Y = north-south distances.

Figure 5.4.1-4. Contour Plots of Waste-Package Temperature for Six Times in the Higher-Temperature Operating Mode Repository

C37

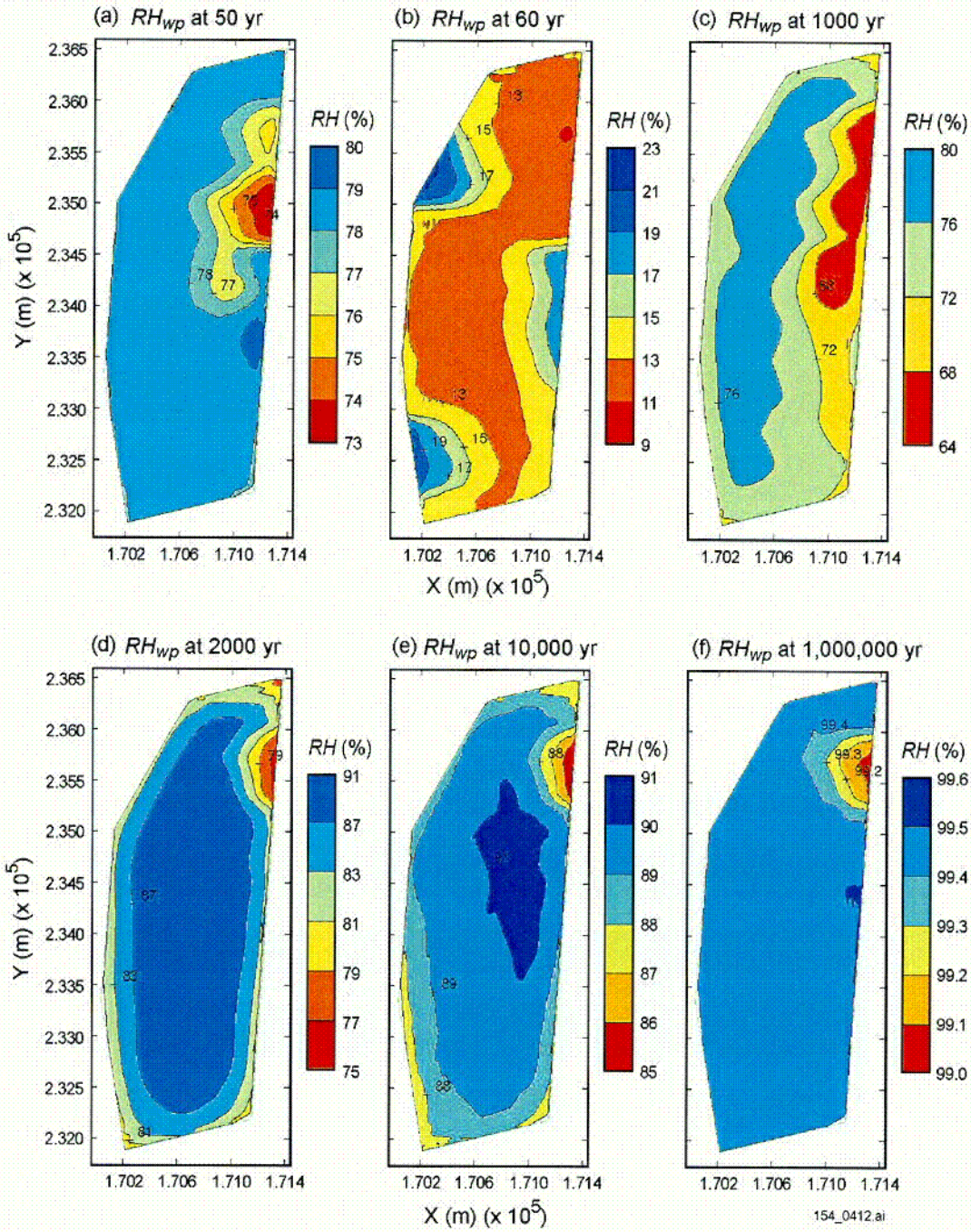

154_0412.ai

Source: Produced using files from Buscheck 2001 [DIRS 155243].

NOTE: Average 21-PWR waste package Mean-infiltration-flux scenario. RH_{WP} = waste package relative humidity, X = east-west distances, Y = north-south distances.

Figure 5.4.1-5. Contour Plots of Waste-Package Relative Humidity at Six Times for the Higher-Temperature Operating Mode Repository

C38

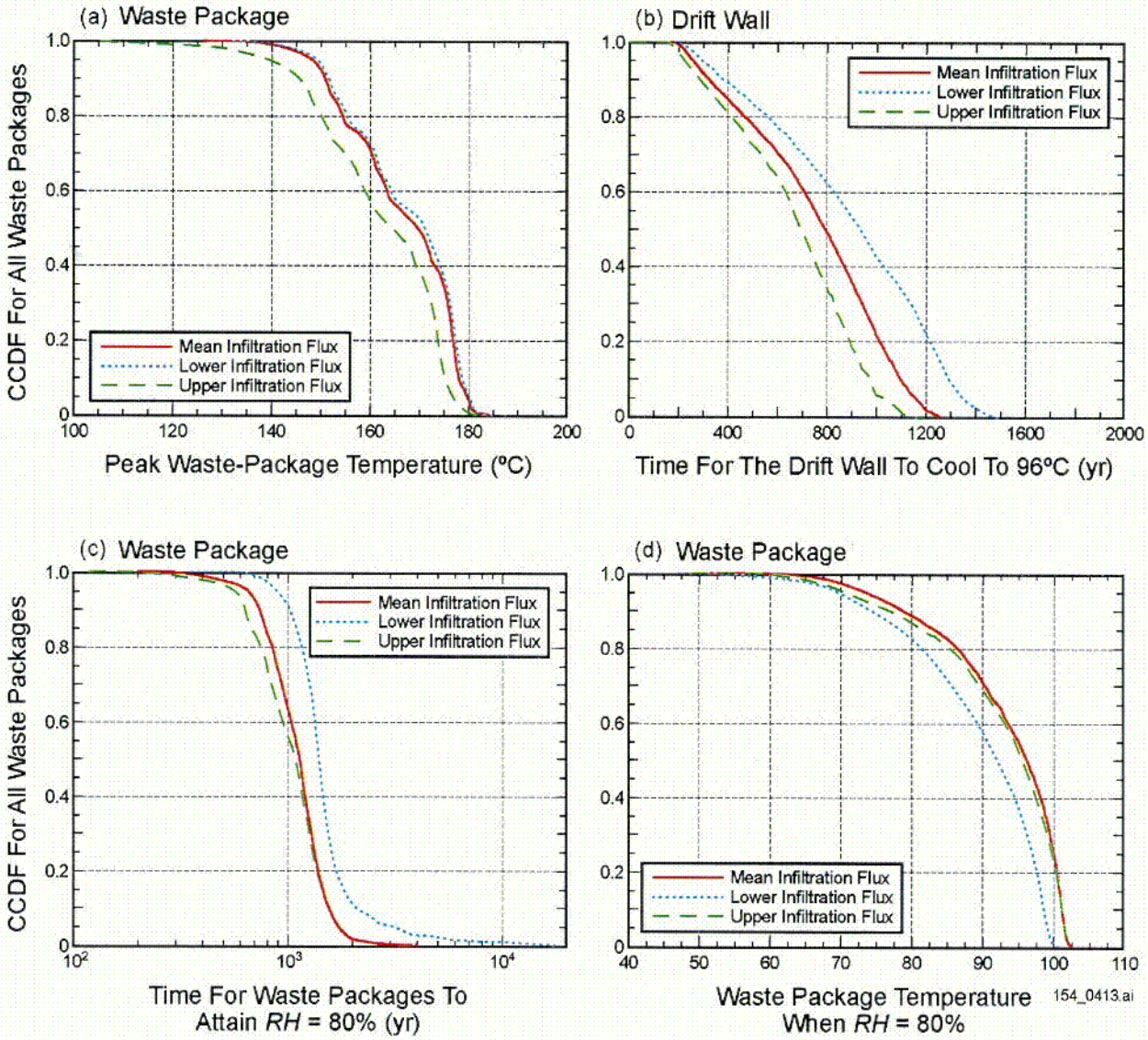

154_0413.ai

Source: Produced using files from Buscheck 2001 [DIRS 155243].

NOTE: CCDF = complementary cumulative distribution function.

Figure 5.4.1-6. Complementary Cumulative Distribution Function of Temperature and Relative Humidity Conditions on the Drift Wall and Waste Package for the Higher-Temperature Operating Mode Repository

C39

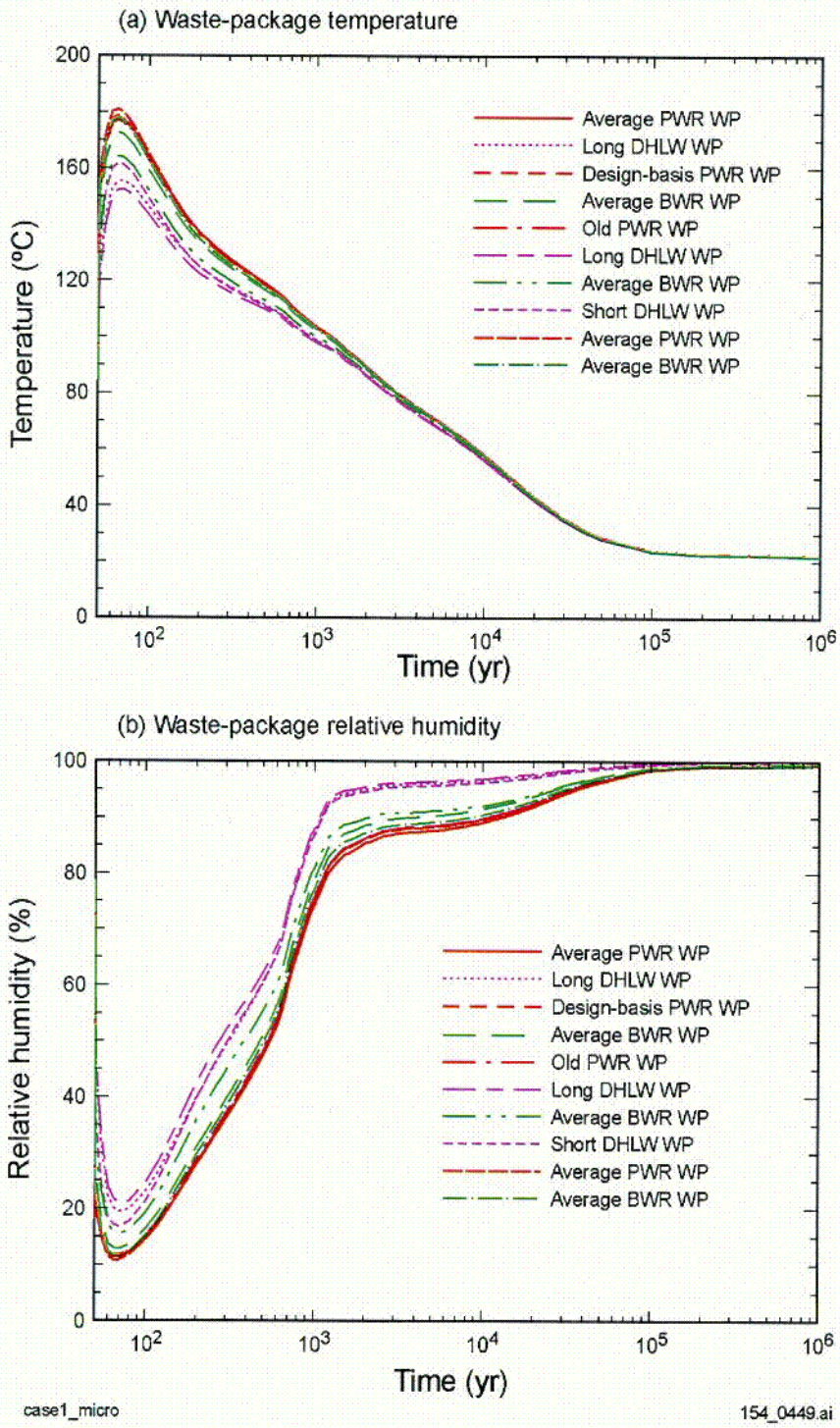

154_0449.ai

Source: Produced using files from Buscheck 2001 [DIRS 155243].

NOTE: Curves are for the 10 waste packages considered in MSTH model calculations at the L5C3 location and the mean-infiltration-flux scenario.

Figure 5.4.1-7. Temperature and Relative Humidity Histories for the Higher-Temperature Operating Mode Predicted by the Multiscale Thermal-Hydrologic Model

C40

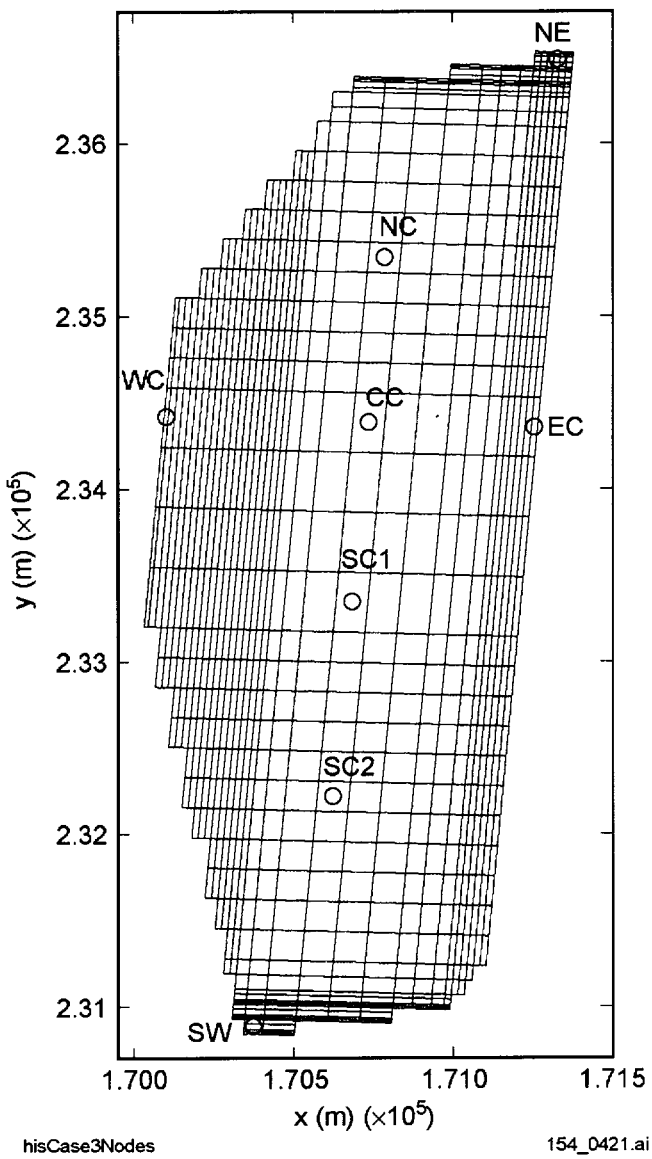

154_0421.ai

Source: Produced using files from Buscheck 2001 [DIRS 155243].

NOTE: Plan view of the potential lower-temperature operating mode repository showing the geographic locations considered in various analyses. X = east-west distances, Y = north-south distances.

Figure 5.4.2-1. Location of Eight Sites Used in Analyses of the Potential Lower-Temperature Operating Mode Repository

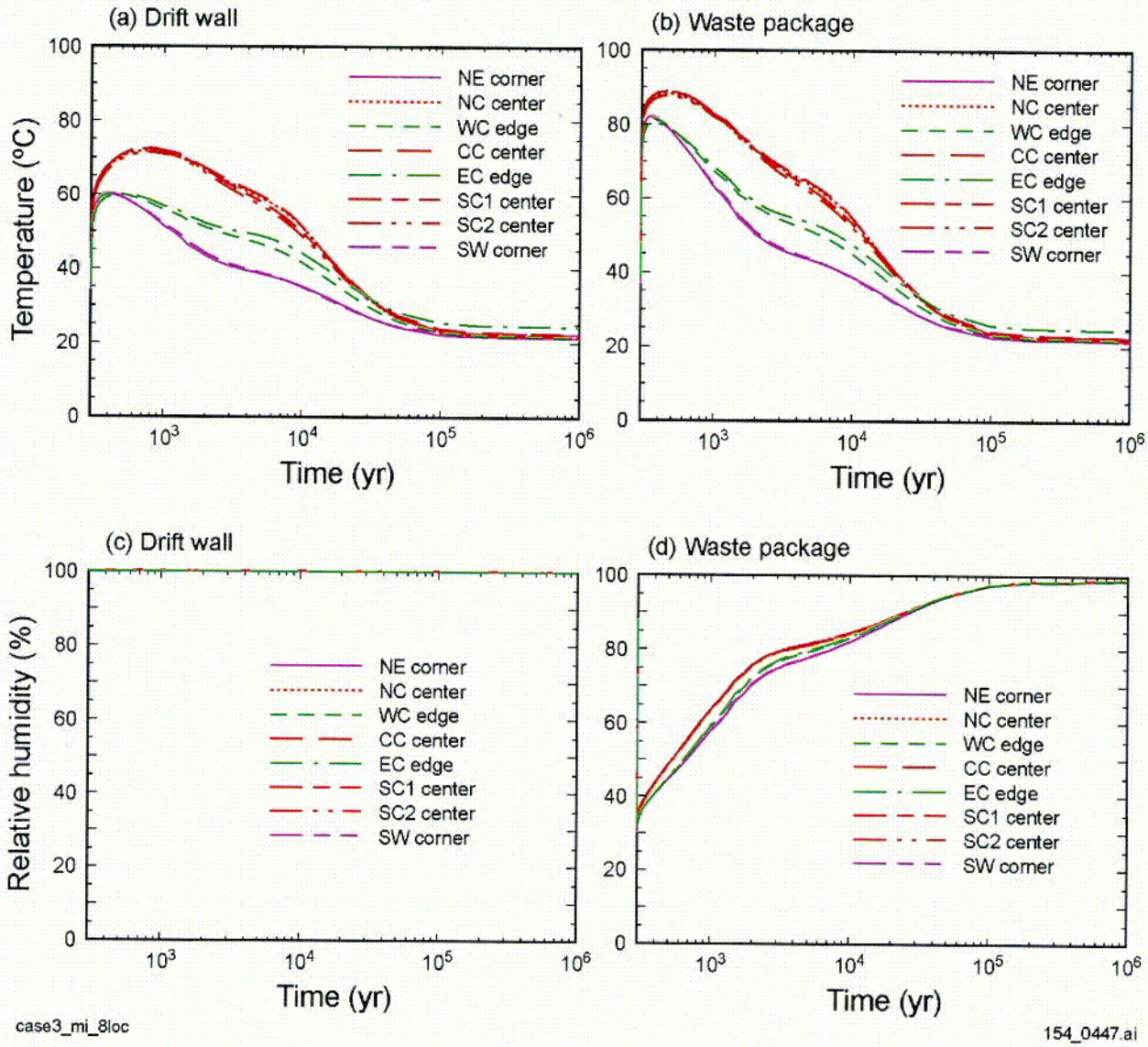

154_0447.ai

Source: Produced using files from Buscheck 2001 [DIRS 155243].

NOTE: Average 21-PWR CSNF waste package Mean-infiltration-flux scenario.

Figure 5.4.2-2. Temperature and Relative Humidity Histories on the Drift Wall and on the Waste Package for Eight Locations in the Potential Lower-Temperature Operating Mode Repository

C41

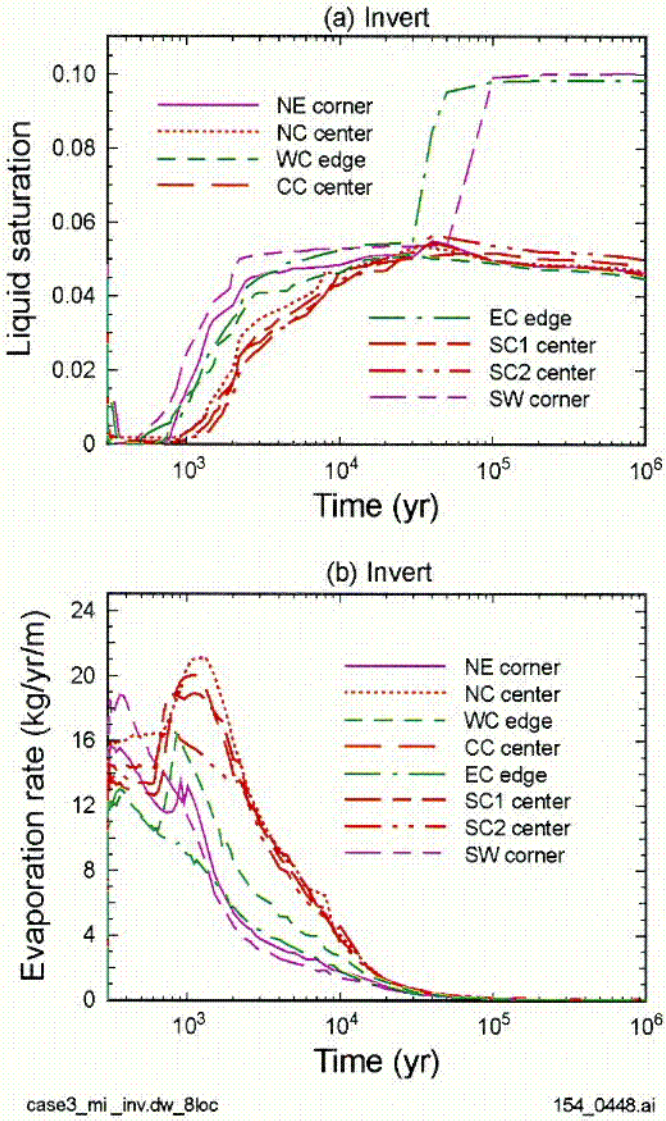

154_0448.ai

Source: Produced using files from Buscheck 2001 [DIRS 155243].

NOTE: Average 21-PWR CSNF waste Mean-infiltration-flux scenario.

Figure 5.4.2-3. Liquid Saturation and Evaporation Rate Histories in the Invert for Eight Locations in the Potential Lower-Temperature Operating Mode Repository

C42

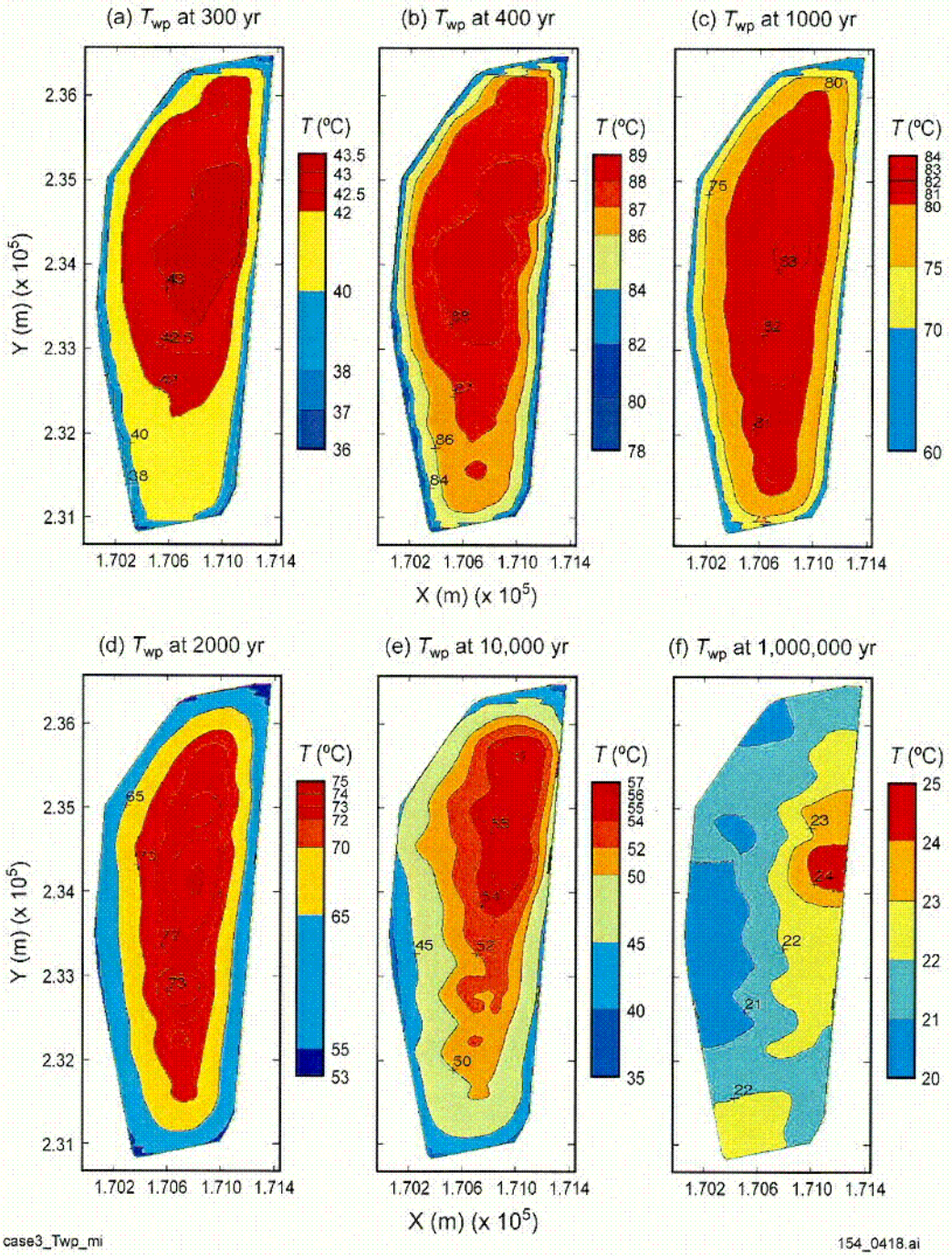

154_0418.ai

Source: Produced using files from Buscheck 2001 [DIRS 155243].

NOTE: Average 21-PWR waste package Mean-infiltration-flux scenario. T_{WP} = waste package temperature, X = east-west distances, Y = north-south distances.

Figure 5.4.2-4. Contour Plots of Waste-Package Temperature for Six Times in the Lower-Temperature Operating Mode Repository

C43

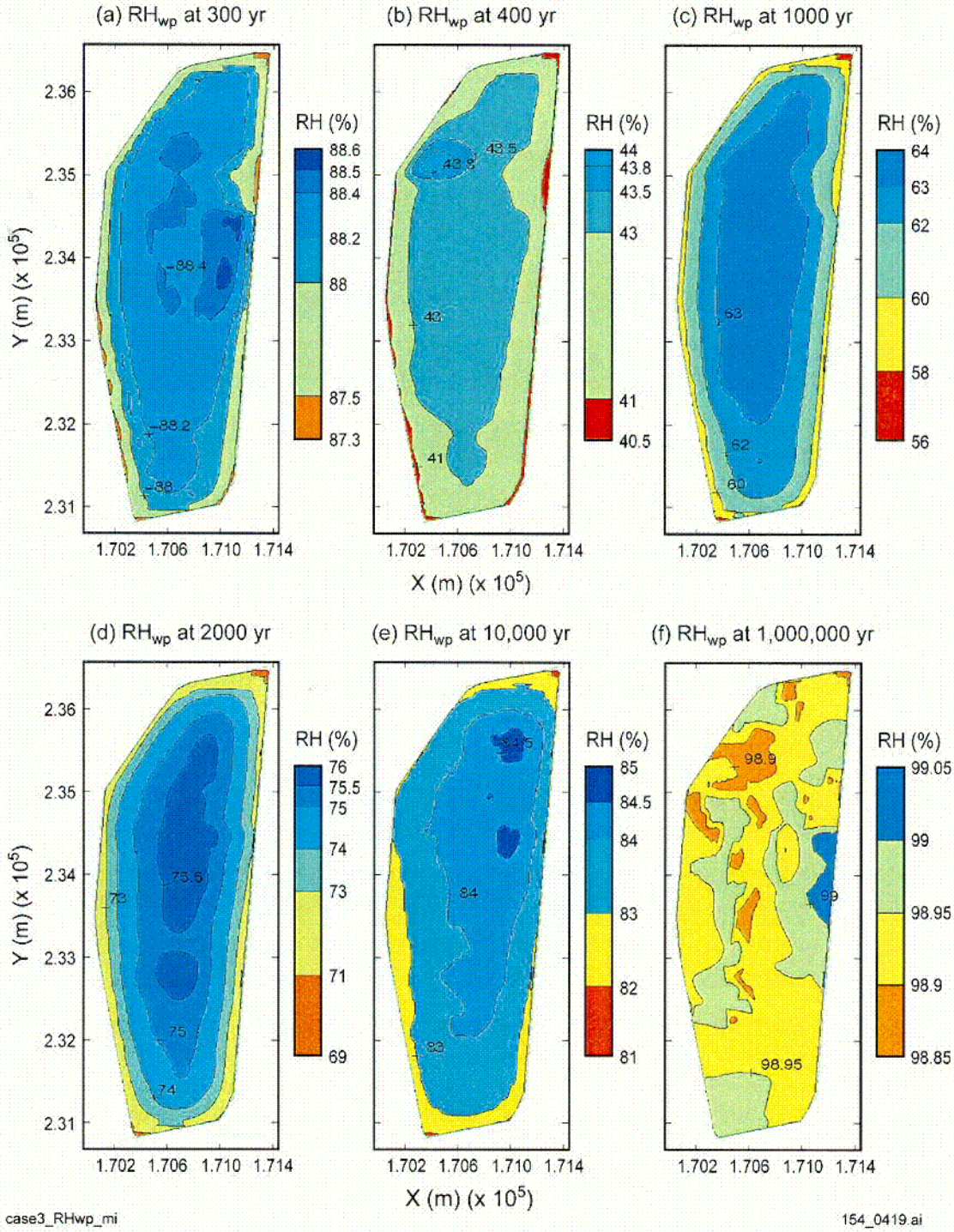

154_0419.ai

Source: Produced using files from Buscheck 2001 [DIRS 155243].

NOTE: Average 21-PWR waste package Mean-infiltration-flux scenario. RH_{WP} = waste package relative humidity, X = east-west distances, Y = north-south distances.

Figure 5.4.2-5. Contour Plots of Waste-Package Relative Humidity at Six Times for the Lower-Temperature Operating Mode Repository

C44

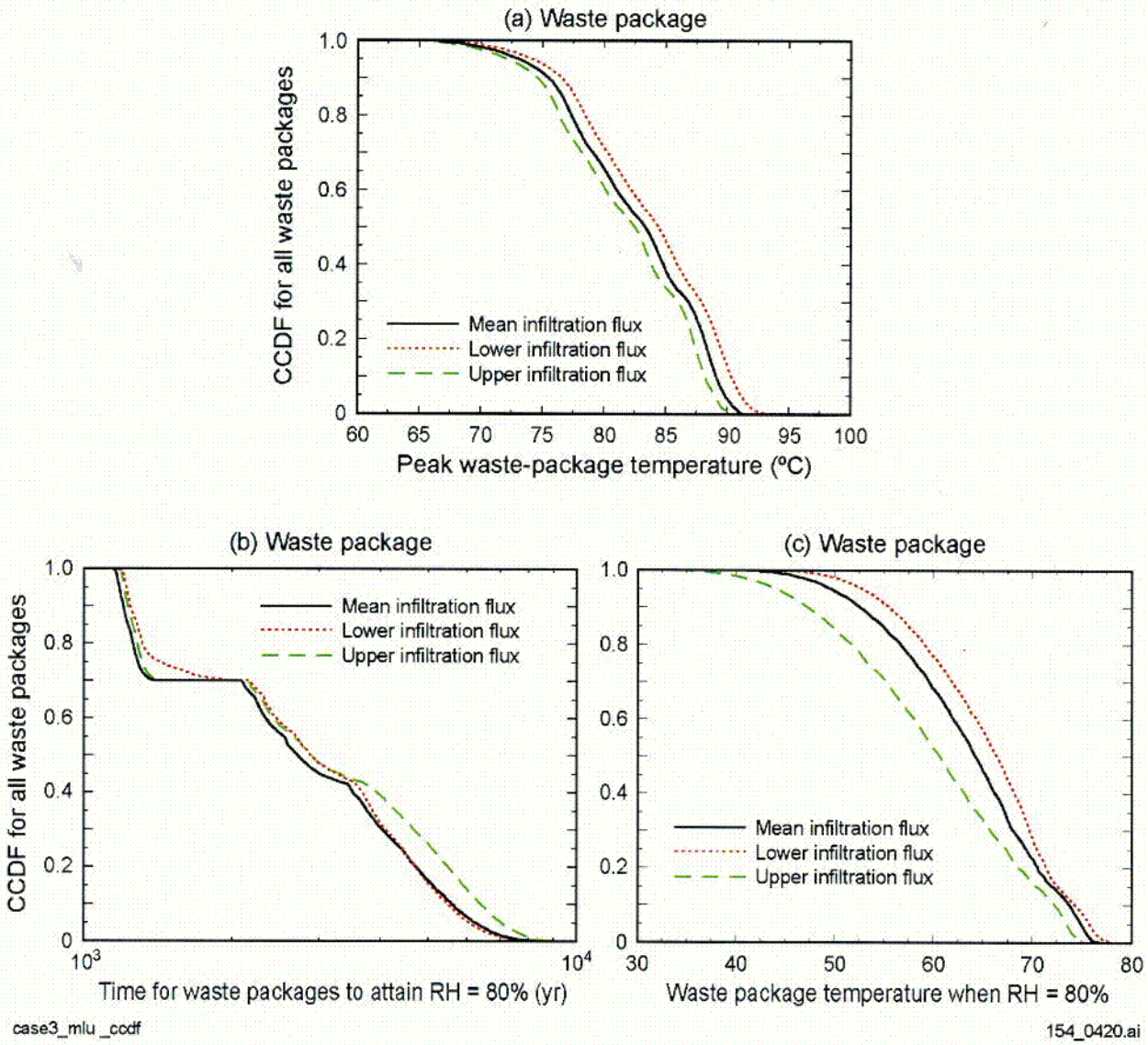

154_0420.ai

Source: Produced using files from Buscheck 2001 [DIRS 155243].

NOTE: CCDF = complementary cumulative distribution function.

Figure 5.4.2-6. Complementary Cumulative Distribution Function of Temperature and Relative Humidity Conditions on the Waste Package for the Potential Lower-Temperature Operating Mode Repository

C45

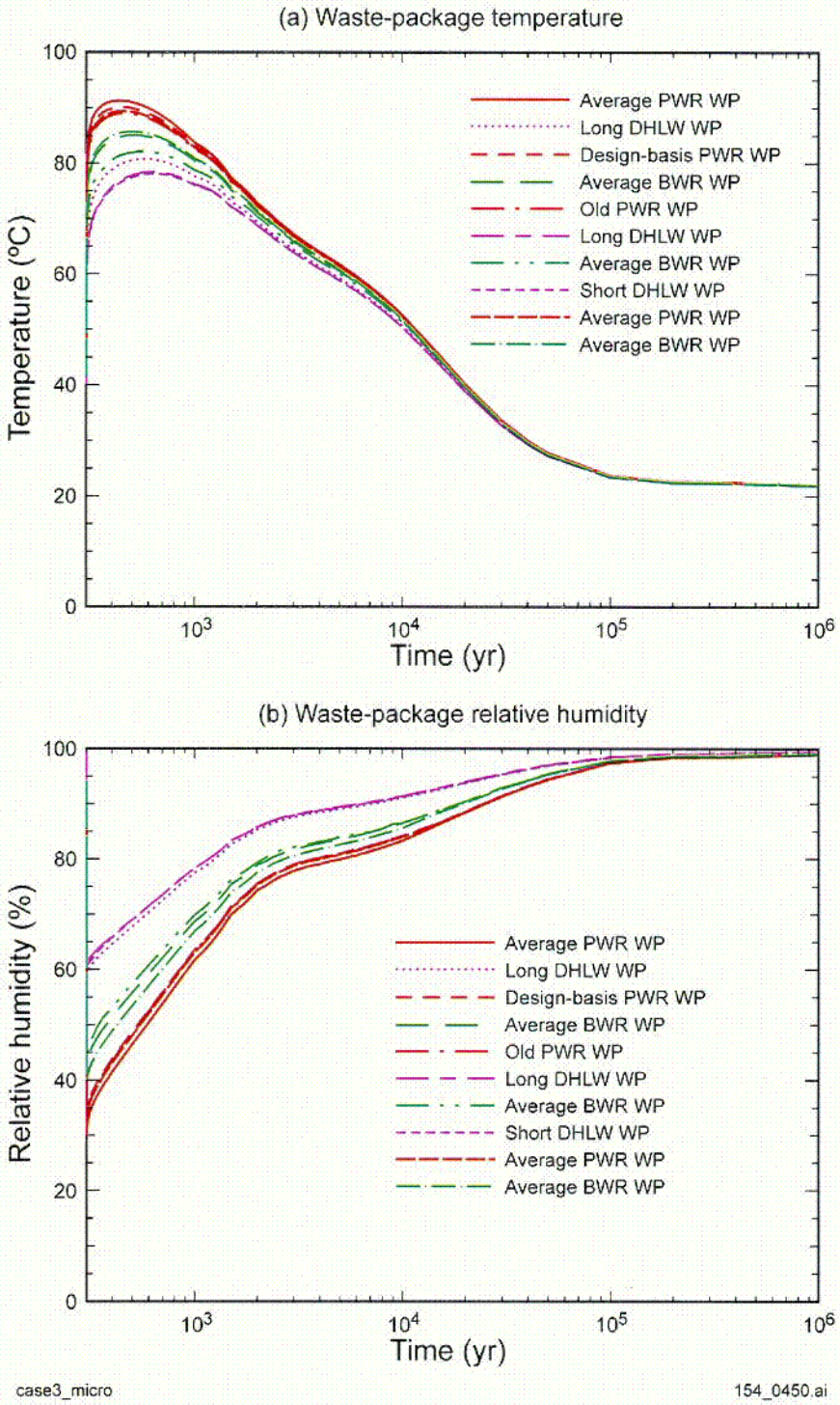

154_0450.ai

Source: Produced using files from Buscheck 2001 [DIRS 155243].

NOTE: Curves are for the 10 waste packages considered in the MSTH model calculations at the L5C3 location for the Mean-infiltration-flux scenario.

Figure 5.4.2-7. Temperature and Relative Humidity for the Lower-Temperature Operating Mode, Histories Predicted by the Multiscale Thermal-Hydrologic Model

c46

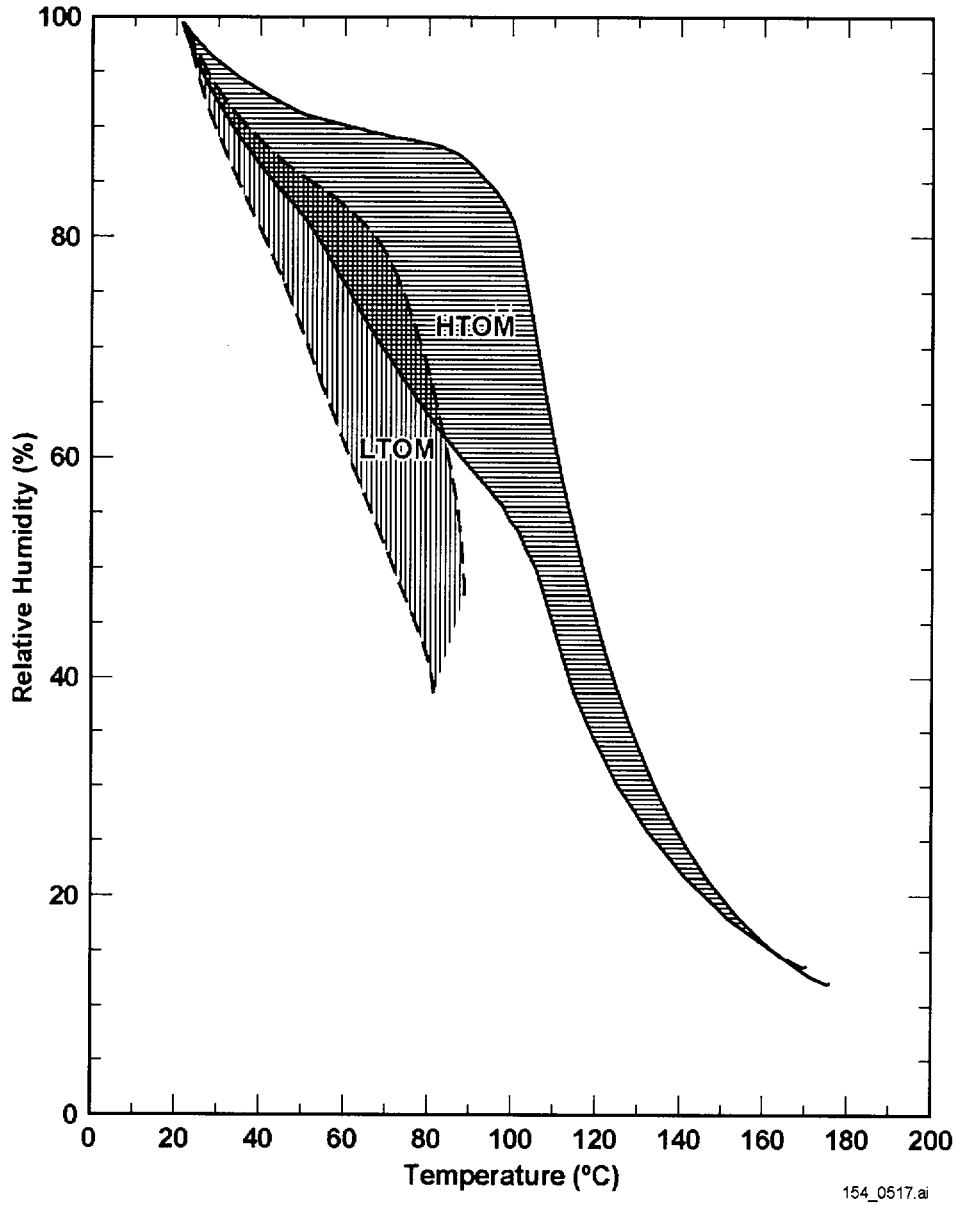

case1case3_mi_T-RH_wp

154_0517.ai

Source: Produced using files from Buscheck 2001 [DIRS 155243].

Figure 5.4.2-8. Thermal-Hydrologic Parameter Evolution for the Higher- and Lower-Temperature Operating Modes